An experimental investigation of the planar turbulent wake in constant pressure gradient

Xiaofeng Liu, Flint O. Thomas,[a] and Robert C. Nelson
Hessert Center for Aerospace Research, The University of Notre Dame, Notre Dame, Indiana 46556

(Received 27 August 2001; accepted 10 May 2002; published 2 July 2002)

This paper describes an experimental investigation into the development of a planar turbulent wake under constant adverse and favorable pressure gradient conditions. The focus of the study is on the near-wake due to its relevance to high-lift systems for commercial transport aircraft. The wake is generated by a flat splitter plate with tapered trailing edge. The pressure gradients are imposed as the wake passes through a wind tunnel diffuser test section with fully adjustable top and bottom wall contours. The streamwise pressure gradients imposed on the wake flow field are held constant in each case. The wake initial conditions are maintained identical upstream of the location where the pressure gradient is first imposed. The use of constant pressure gradients, coupled with identical initial conditions, facilitates isolation of the effect of streamwise pressure gradients on the near-field evolution of the wake and provides a clean test case for computational models. In this paper we focus on characterizing the mean flow widening, streamwise velocity defect variation, and the streamwise evolution of turbulence statistics for both favorable and adverse streamwise pressure gradients. The imposed pressure gradients are shown to have a very significant effect on both the mean and turbulent flow quantities. © *2002 American Institute of Physics.*
[DOI: 10.1063/1.1490349]

I. BACKGROUND AND MOTIVATION

This paper presents the results of an experimental investigation into the development and structure of a planar turbulent wake exposed to *constant* favorable and adverse pressure gradients. Although the study is motivated by its relevance to high-lift systems for commercial transport aircraft, it is also of interest from a fundamental standpoint since it involves a turbulent free shear flow exposed to well-defined streamwise straining.

In multielement wings used for commercial transport aircraft, the wake generated by each forward element will inevitably develop in a strong pressure gradient environment, and subsequently interact with downstream elements. The nature of this interaction will depend critically on the wake's response to the imposed pressure field. For example, the spreading rate of the leading edge slat wake will determine, in part, the location of onset of confluence with the main element boundary layer. Even in cases where there is no strong confluence on the main element, the slat wake will have the effect of moderating the surface pressure peak on the trailing flap(s). The degree of flap surface pressure peak moderation (and consequently, flap flow attachment) is directly related to the wake width as described by Garner, Meredith, and Stoner.[1] In general, the thicker the wake, the more the flap surface pressure peak is moderated due to the associated streamline displacement effect. Another example of the influence of wake spreading on high-lift system performance is apparent from the experimental study of Lin, Robinson, and McGhee.[2] They explored the effect which sub-boundary layer scale vortex generators placed on the trailing flap surface of a multielement airfoil had on flap flow attachment. As expected, the vortex generators were found to augment lift at low-to-moderate angles of attack. Surprisingly, however, their results showed no benefit at high attack angles where it was found that flow attachment was maintained even without the use of vortex generators. This appears due to the fact that at the highest incidence angles prior to stall, the main element wake thickens quite dramatically in response to the imposed pressure gradient which has the effect of suppressing the trailing flap surface pressure peak. As a consequence, the flap boundary layer flow remains attached. In contrast, at low angles of attack the wake is comparatively thin and less effective at moderating the flap surface pressure peak.

In addition to issues related directly to wake spreading, Smith[3] notes that off-surface flow reversal can occur if a wake encounters a sufficiently strong adverse pressure gradient. This has been termed by some as ''wake bursting.'' There has been speculation that wake bursting may be responsible, in part, for the so-called ''inverse Reynolds number effects'' in high-lift systems in which the maximum lift performance will unexpectedly degrade with increased Reynolds number. Wake bursting in a strong adverse pressure gradient was demonstrated in the experiments of Hill, Schaub, and Senoo.[4] The existence of off-surface flow reversal of the wake generated by an upstream element of a multielement airfoil was detected visually by Petrov.[5] In addition, some measurements from the low turbulence pressure tunnel at NASA Langley (e.g., Chin *et al.*[6]) show wake pro-

[a]Electronic mail: Flint.O.Thomas.1@nd.edu

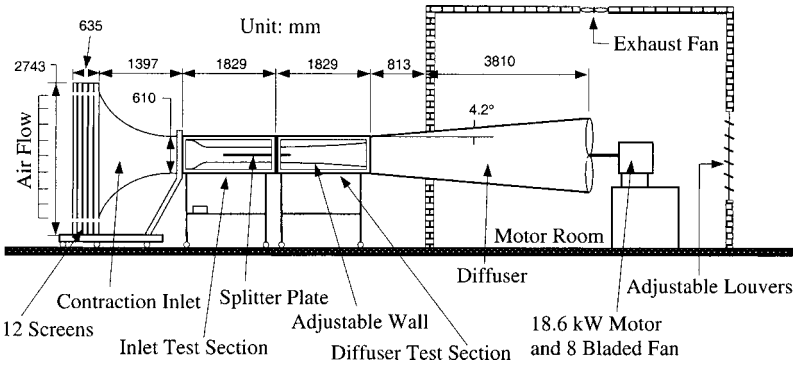

FIG. 1. Schematic of the subsonic wind tunnel facility and wake test section.

files over the trailing edge flap of a Douglas three-element high-lift system that appear very close to exhibiting off-surface reversal. High-lift aerodynamic computations by Rogers[7] clearly show reversed wake flow over a multielement airfoil trailing flap. Hoffenberg, Sullivan, and Schneider[8] and Hoffenberg and Sullivan[9] applied an adverse pressure gradient of sufficient strength (by means of a planar diffuser) to cause flow reversal to occur. Tummers, Passchier, and Henkes[10] investigated the wake of a flat plate subjected to an adverse pressure gradient that resulted in local flow reversal. Roos[11] used passive flow control of the boundary layer on a splitter plate in order to form an initially asymmetric wake profile which was then exposed to a strong adverse pressure gradient. It was clearly demonstrated that the initial wake asymmetry plays an important role in the subsequent wake development. That is, initially symmetric and asymmetric wakes will respond quite differently to a given imposed pressure gradient. More recently, a comprehensive experimental investigation of pressure gradient induced flow reversal of a symmetric turbulent wake at high Reynolds number was completed by Driver and Mateer.[12]

In addition to its relevance to high-lift aerodynamics, the turbulent wake in pressure gradient has also received considerable attention as a prototypical free turbulent shear flow exposed to streamwise straining. The focus of most previous studies has typically been on the asymptotic response of turbulent wakes in spatially varying pressure gradients or the relaxation process by which an equilibrium wake responds to impulse-like pressure perturbations. For example, Narasimha and Prabhu[13] and Prabhu and Narasimha[14] investigated the asymptotic response of an equilibrium turbulent wake to a nearly impulsive pressure perturbation. They showed that the approach to a new equilibrium state is exponential, with a relaxation length scale on the order of 10^3 momentum thicknesses. Studies by Reynolds[15] and Keffer[16] indicate that when constant rates of strain are applied to turbulent wakes, the flow is seldom truly self-preserving even though the governing equations of the mean motion may admit to self-preserving solutions. Gartshore[17] showed that the two-dimensional turbulent wake can be self-preserving only when it is subjected to an appropriately tailored pressure gradient. Nakayama[18] studied the combined effects of mild pressure gradient and streamline curvature on a two-dimensional, low momentum deficit turbulent wake. More recently, direct numerical simulations (DNS) of a temporally evolving, strained planar turbulent wake were undertaken by Rogers[19] using a pseudospectral method. It was noted that despite a lack in complete similarity, the wake velocity defect profile was nearly universal. The response of the mean flow to the imposed strain fields was rapid but that of the turbulence significantly slower. In fact, the turbulent field was found not to keep pace with the mean flow even for low strain rates.

II. OBJECTIVES

As described in Sec. I, the flow physics associated with wake development in pressure gradients has been studied in the past, although the focus has often been on the asymptotic behavior in complex pressure gradient environments. Other studies have focused upon the response of wakes to adverse gradients of sufficient magnitude to give rise to wake flow reversal. In contrast, this study will examine the response of a symmetric turbulent planar wake to imposed *constant* favorable and adverse streamwise pressure gradients. The work is motivated by the need to understand and accurately predict the effect of pressure gradient on near-wake development. The focus on near-wake behavior is motivated by its relevance for high-lift applications. Another unique aspect of this study is that in each case the wake initial conditions are maintained to be identical upstream of the imposition of the pressure gradient. The use of constant pressure gradients, coupled with identical initial conditions, creates a very ''clean'' experiment for isolating the effect of streamwise pressure gradients on the near-field evolution of the wake and for providing a test case for computational models. In this paper we are particularly interested in characterizing the mean flow spreading, streamwise velocity defect variation, and the streamwise evolution of turbulence statistics for both favorable and adverse streamwise pressure gradients.

III. EXPERIMENTAL FACILITY AND MEASUREMENT APPARATUS

A. Flow field facility

The experiments were performed in an open-return subsonic wind tunnel facility located at the Hessert Center for Aerospace Research at the University of Notre Dame. A schematic of the wind tunnel facility is shown in Fig. 1. Ambient laboratory air is drawn into a 2.74 m by 2.74 m inlet contraction by an eight-bladed fan connected to an 18.6

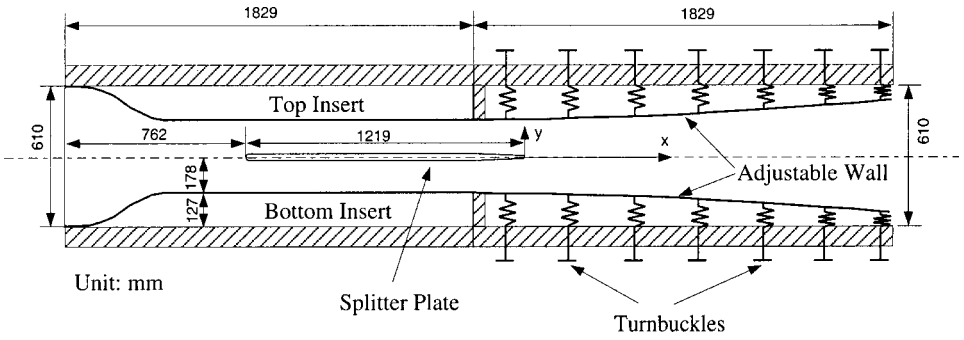

FIG. 2. Schematic of the test section (all units in mm).

kW ac induction motor. The contraction ratio of the tunnel inlet is 20.25:1. The inlet contains 12 turbulence reduction screens that yield a very uniform test section velocity profile with a free stream fluctuation intensity level that is less than 0.1% (and less than 0.06% for frequencies greater than 10 Hz).

For these experiments the wind tunnel utilizes two consecutive test sections, both of which were specifically constructed for the wake development study. The upstream test section contains a wake-generating splitter plate while the second forms a diffuser section as shown in Figs. 1 and 2. The wake measurements were conducted in the diffuser section which is used to produce the desired adverse/favorable pressure gradient environment.

The upstream test section is 1.83 m in length, 0.61 m in width, and 0.36 m in height. The length and the width of the diffuser section are the same as those of the upstream test section. The top and bottom walls of the diffuser are made of sheet metal and their contour is fully adjustable by means of seven groups of turnbuckles in order to create the desired constant pressure gradient environment. To facilitate flow visualization and laser Doppler velocimetry (LDV) measurement, both test sections have one sidewall made of plate glass. As indicated in Fig. 2, x, y, and z denote the streamwise, lateral (cross-stream), and spanwise spatial coordinates, respectively.

The wake generating body is a Plexiglas™ splitter plate with a chord length of 1.22 m and a thickness of 17.5 mm. The leading edge consists of a circular arc with distributed roughness which gives rise to turbulent boundary layers which develop over the top and bottom surfaces of the plate. The last 0.2 m of the plate consists of a 2.2° linear symmetric taper down to a trailing edge of 1.6 mm thickness. The splitter plate model is sidewall mounted in the test section with end plates used to minimize the influence of tunnel sidewall boundary layers. For additional details regarding the wake generating body and flow field facility, the reader is referred to Liu, Thomas, and Nelson.[20]

Measurement of the streamwise surface pressure distribution over the plate (via an array of static taps) shows that the splitter plate boundary layer develops under a very slight favorable streamwise pressure gradient condition due to the boundary layer growth on both the plate surface and the tunnel walls. Measurements of the spanwise surface pressure distribution on the plate (not presented) show that it is uniform to within 1.5%. In addition, LDV boundary layer surveys obtained at selected fixed streamwise but different spanwise locations on the splitter plate were found to be identical. This indicates that the flow over the plate is two-dimensional in the mean.

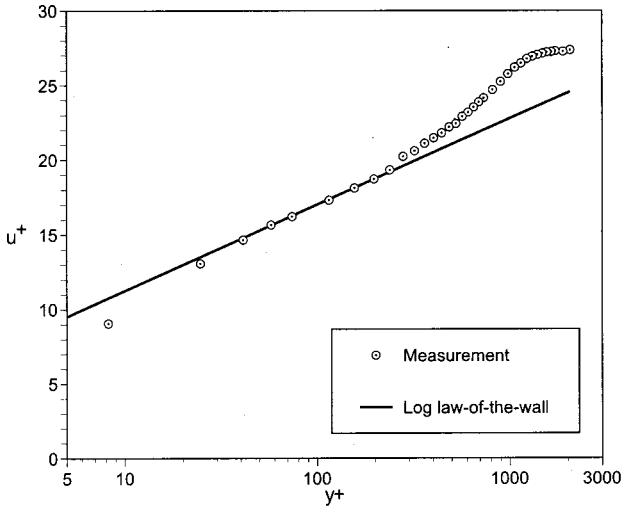

(a)

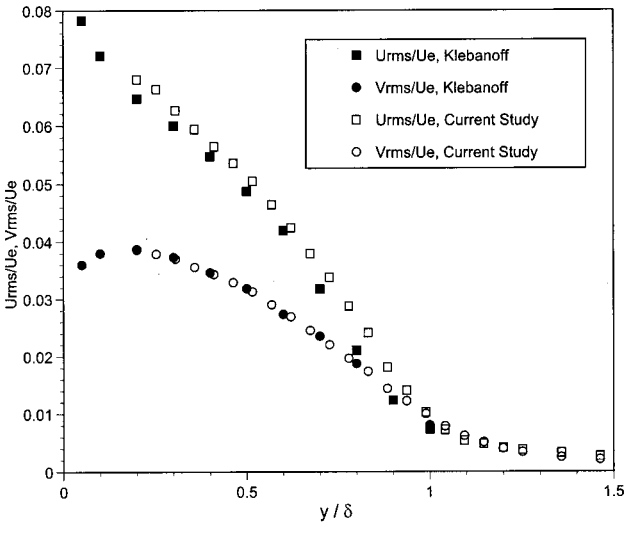

(b)

FIG. 3. (a) Inner variable scaling of the boundary layer mean velocity profile at the 75% chord location on the splitter plate; (b) comparison of X-wire u- and v-component turbulence intensity measurements at $x/c=75\%$ on the splitter plate with the data of Klebanoff (Notre Dame wake study: $\mathrm{Re}_\delta = 5.0\times10^4$; Klebanoff: $\mathrm{Re}_\delta = 7.8\times10^4$).

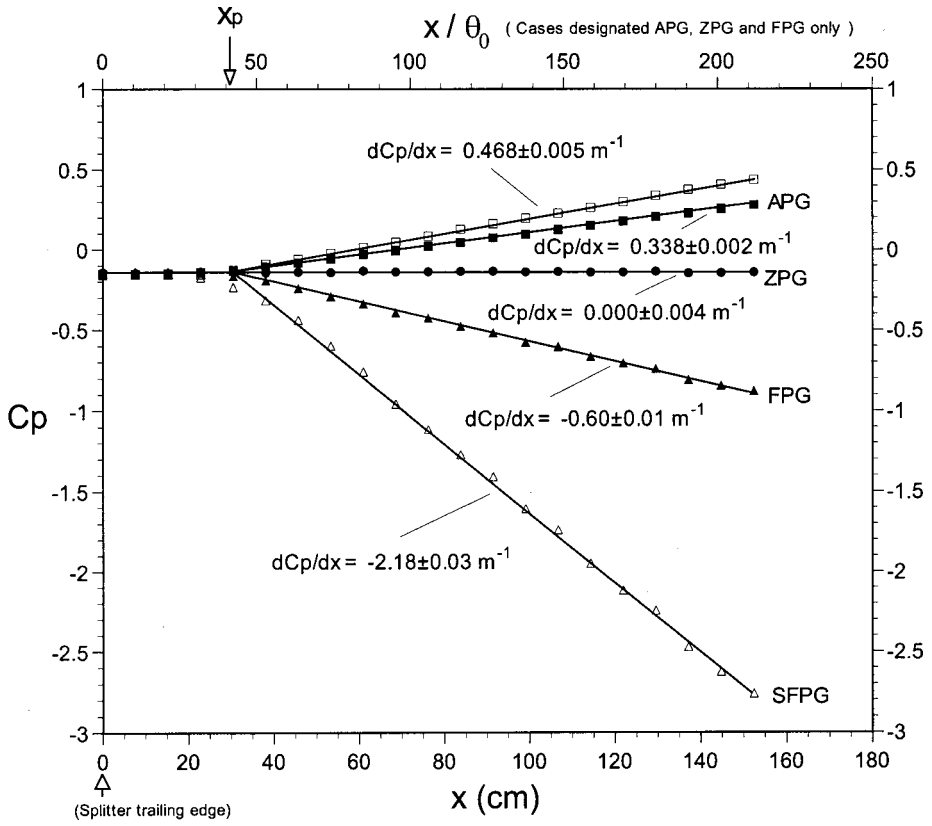

FIG. 4. Measured pressure distributions for zero, adverse, and favorable pressure gradient cases.

Figure 3 presents an example of the plate boundary layer mean velocity and turbulence intensity profiles measured at the 75% chord location. From Fig. 3(a) it can be seen that the splitter plate boundary layer exhibits classic log law-of-the-wall behavior. Although not presented here, similar mean flow behavior was observed at stations extending to the 99.9% chord location. The boundary layer streamwise and wall normal-component turbulence intensity profiles are shown in Fig. 3(b) along with the results of Klebanoff.[21] The two data sets are observed to be in good agreement.

B. Imposed streamwise pressure gradients

The streamwise pressure distribution was measured by means of a series of pressure taps located on one flat sidewall of the diffuser test section at the same lateral (i.e., y) location as the centerline of the wake. Laser Doppler velocimetry-based measurements of the centerspan streamwise distribution of mean velocity, $U(x)$, were found to be fully consistent with the measured wall pressure variation, thereby confirming the suitability of the pressure tap placement and use in the characterization of the imposed pressure field. In this paper the imposed pressure will be expressed in terms of a pressure coefficient, $C_p=(P(x)-P_\infty)/q_\infty$, where $P(x)$ is the local static pressure in the diffuser, P_∞ and q_∞ are the static and dynamic pressures, respectively, upstream of the splitter plate.

Four sets of experiments were conducted: (1) a zero pressure gradient (ZPG) base flow condition, $dCp/dx=0.0\ \mathrm{m}^{-1}$; (2) a constant adverse pressure gradient (APG) condition with $dCp/dx=0.338\ \mathrm{m}^{-1}$; (3) a moderate constant favorable pressure gradient (FPG) condition with $dCp/dx=-0.60\ \mathrm{m}^{-1}$; and (4) a more severe constant favorable pressure gradient (SFPG) $dCp/dx=-2.18\ \mathrm{m}^{-1}$. The zero pressure gradient wake served both as an essential baseline case for comparison with the nonzero pressure gradient wake development and as a means to further validate the flow field facility.

The measured streamwise pressure distributions corresponding to these different experimental conditions are shown in Fig. 4. Also shown in Fig. 4 is a larger adverse pressure gradient case that was run but found to give rise to intermittent, unsteady flow separation near the aft portion of the diffuser wall. Wake measurements for this case will not be presented. This case is included in Fig. 4 since it may be regarded as an effective upper limit on the magnitude of the constant adverse pressure gradient that can be produced by the diffuser without incurring intermittent unsteady flow separation effects. The imposition of a constant adverse dC_p/dx is associated with a "trumpet shaped" diffuser wall contour. Thus for large constant adverse pressure gradients the wall slope can become excessive at the farthest downstream stations. Since unsteady effects associated with intermittent diffuser wall separation were to be avoided, this required that the magnitude of the imposed adverse gradients be kept modest. Fortunately, as will be shown in this paper, the wake's response to even modest gradients produce quite significant changes in the global behavior of the near wake. The Appendix tabulates the diffuser wall coordinates corresponding to each of the pressure gradient cases shown in Fig. 4.

For each pressure gradient case shown in Fig. 4, note that a common zero pressure gradient zone occurs immedi-

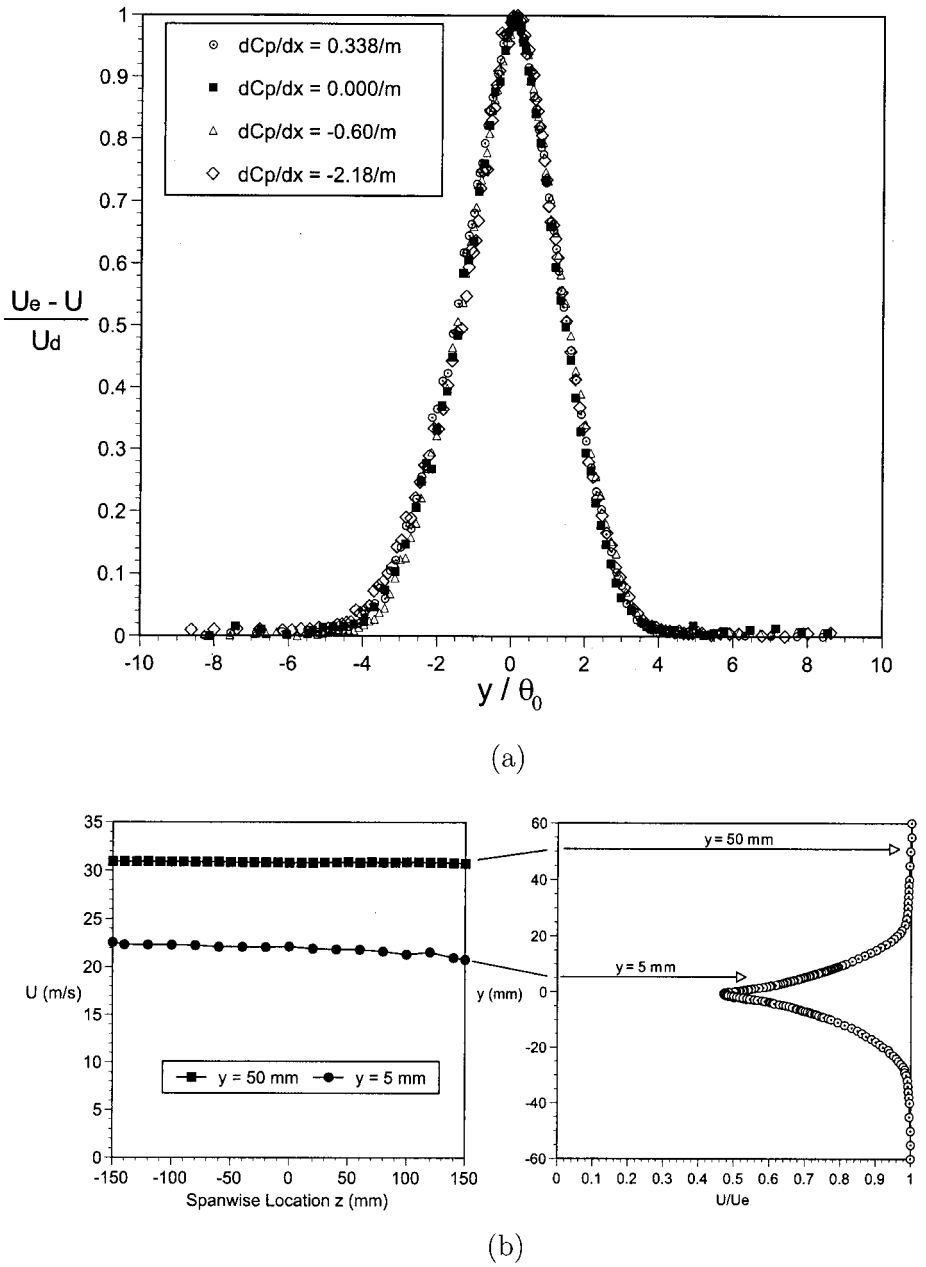

FIG. 5. (a) Comparison of initial wake mean velocity profiles at $x/\theta_0=18$ measured via LDV; (b) example spanwise mean velocity distribution at $x/\theta_0=2.6$.

ately downstream of the splitter plate trailing edge in order to ensure that the wake initial condition is identical in each case. Figure 5(a) confirms that the initial wake mean velocity profiles are virtually identical for each of the experimental conditions. In this figure θ_0 is the initial wake momentum thickness, U_e is the local velocity outside the wake, and U_d denotes the local maximum velocity defect. Maintenance of the same wake initial condition in conjunction with the use of a constant dC_p/dx facilitated isolation of the effect of pressure gradient on the near-wake development.

Before conducting the detailed flow field surveys for the different pressure gradient cases, the quality of the flow field in the diffuser test section was carefully examined. These measurements verified the two-dimensionality of the flow field in the mean. As an example, Fig. 5(b) shows the spanwise distribution of the mean streamwise velocity component at two different y locations within the initial wake. It should be pointed out that the slight spanwise variation of the mean velocity U at the location $y=5$ mm was traced to a slight misalignment of the traverse system with the wind tunnel coordinates rather than an actual spanwise variation of the flow field itself. Measurement of the spanwise variation of the wake at different streamwise stations located farther downstream reveal that the mean flow two-dimensionality of the wake remains quite satisfactory in the diffuser test section up to the last measurement station at $x=1.52$ m.

C. Flow field parameters

The experiments were performed at a Reynolds number of $\mathrm{Re}=2.4\times10^6$ (based on the chord length of the splitter plate and a free stream velocity of $U_{e0}=30$ m/s) for all cases except the SFPG case, which corresponds to a Reynolds number $\mathrm{Re}=2.0\times10^6$ (with a free stream velocity of U_{e0}

$=24$ m/s). As a basis for comparison, it may be noted that a Boeing 737-100 operating at a mean chord Reynolds number of 15.7×10^6 during landing approach will have a Reynolds number based on slat chord of about 1.8×10^6, which is quite comparable to this experiment.

For the ZPG, APG, and FPG cases which have the same tunnel speed of 30 m/s the initial wake momentum thickness $\theta_0=7.2$ mm and the Reynolds number (based on initial wake momentum thickness) $\mathrm{Re}_\theta=1.5\times10^4$. However, for the SFPG case the initial wake momentum thickness $\theta_0=8.1$ mm due to a lower initial free stream flow velocity and the corresponding Reynolds number was $\mathrm{Re}_\theta=1.3\times10^4$.

As mentioned earlier, this study will focus on near-wake behavior due to its relevance for high-lift applications. From Fig. 4, it can be seen that the useful length of the test section for the investigation of the wake development extends 1.52 m downstream of the trailing edge of the splitter plate. This streamwise range corresponds to $0<x/\theta_0<212$. Both LDV and hot-wire measurements were performed at the center span location for a variety of selected streamwise positions within the aforementioned range of the diffuser test section.

D. Flow field diagnostics

The development of the wake mean and turbulent velocity field for the selected pressure gradients was investigated nonintrusively with an Aerometrics three-component fiber optic laser Doppler velocimetry system and also with constant temperature hot-wire anemometry. Wherever possible both techniques were employed in order to insure fidelity of the data.

The fiber optic LDV system was typically operated in two-component backscatter mode in order to measure the streamwise velocity component, u, and the cross-stream velocity component, v. The 514.5 and 488 nm laser wavelengths were used to measure the u and v components of velocity, respectively. Frequency shifting was used in order to unambiguously resolve flow direction. The measurements were made in the coincidence mode and results for both mean flow and turbulence quantities presented in this paper represent ensemble averages over at least 10 000 valid coincident LDV burst events. Wind tunnel seeding was performed at the tunnel inlet with an Aerometrics Particle Generator Model APG-100 using a 1:2 mixture of propylene glycol and distilled water. The transceiver of the LDV system was mounted to a computer controlled traverse table. The positioning accuracy of the traverse table in both the horizontal and vertical directions was 0.4 μm. The streamwise and cross-stream dimensions of the measurement probe volume of the LDV system were 234.4 and 234.0 μm, respectively.

The LDV surveys were repeated using constant temperature hot-wire anemometry. In addition, the measurement of certain terms in the wake turbulence kinetic energy budget (not presented in this paper) required the use of hot-wire anemometry techniques. For the reported hot-wire measurements a multichannel TSI IFA 100 anemometer together with X-wire probes (Auspex type AHWX-100) were used. The anemometer output was anti-alias filtered at 10 kHz and digitally sampled at 20 kHz. The total record length at each measurement station was 26.2 s. Comparison between the LDV and X-wire measurements showed excellent agreement in both mean flow and turbulence quantities with the exception of the free stream turbulence intensity values which are overpredicted by the LDV. This is a well-known problem with LDV measurement systems in low-turbulence free stream environments.

IV. EXPERIMENTAL RESULTS

A. Wake mean flow development

In this section experimental results documenting the mean flow development of the wake for the constant pressure gradient cases are presented. Cross-stream wake mean velocity profiles obtained at selected streamwise locations via LDV surveys were used to establish the streamwise variation of the wake mean velocity half-width, $\delta(x)$, and the local maximum velocity defect, $U_d(x)$. Here $\delta(x)$ is defined as the lateral distance from the centerline of the wake to the position at which the local velocity defect drops to one-half $U_d(x)$. For purpose of comparison we also present results for the zero pressure gradient wake which is expected to exhibit well-defined mean flow similarity scaling with sufficient distance downstream of the splitter plate trailing edge. For example, it is well known that the ZPG planar turbulent wake half-width, $\delta(x)$, and the local maximum velocity defect, $U_d(x)$, should vary as $x^{1/2}$ and $x^{-1/2}$, respectively, given sufficient distance downstream of the wake generating body (Schlichting[22]).

Figure 6 presents the measured streamwise variation of the wake mean velocity half-width for zero, favorable, and adverse pressure gradient conditions. Both δ and the streamwise coordinate x are made nondimensional by the initial wake momentum thickness, θ_0. The streamwise location at which the pressure gradient is first applied is indicated on the abscissa as x_p. The profound effect of the pressure gradient on wake spreading is readily apparent from Fig. 6. The baseline zero pressure gradient case is shown to exhibit the expected streamwise growth. In contrast, the adverse pressure gradient case is observed to spread approximately exponentially with x as evidenced by the indicated least-squares fit. It is interesting to note that in the DNS of a turbulent wake by Rogers,[19] the case of constant negative streamwise strain rate exhibited spreading that was approximately exponential in time. More will be said about these DNS results later. In contrast, Fig. 6 shows that for the favorable pressure gradient cases the wake spreading is greatly reduced. The wake width for favorable pressure gradient appears to follow a power law variation with x but with reduced exponent n from the value of $\frac{1}{2}$ that characterizes the zero pressure gradient case. Near the end of the diffuser section, the FPG case appears to be approaching a parallel flow condition ($d\delta/dx\rightarrow0$). Note that for the SFPG case shown in Fig. 6, the wake flow is essentially parallel with $\delta\approx$const. Recall that θ_0 for this case is larger so that the scaled x coordinate is shifted with respect to the other three cases.

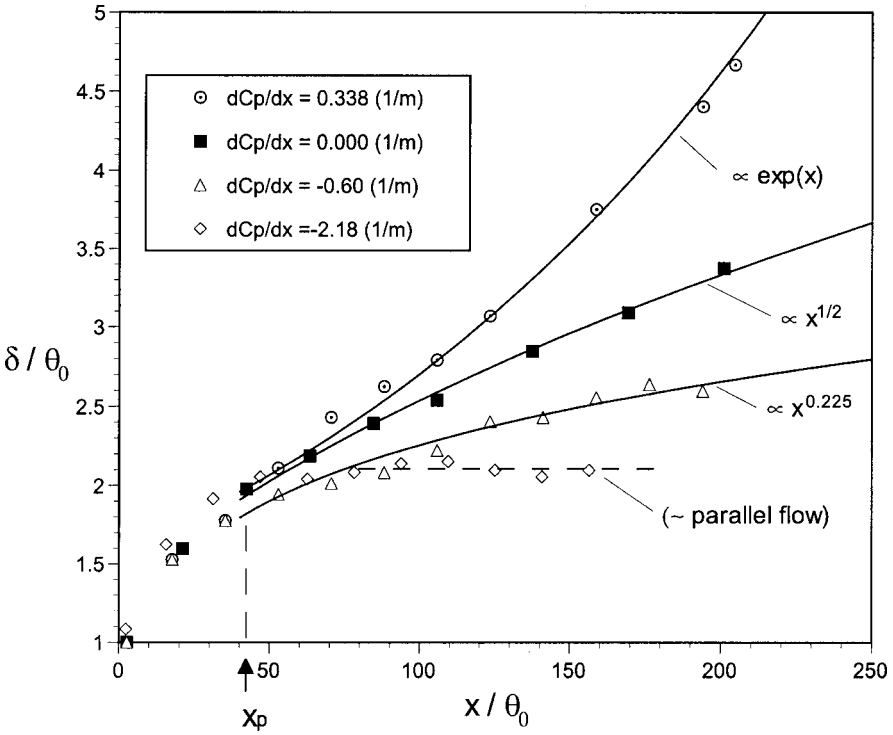

FIG. 6. Streamwise variation of wake half-width for different pressure gradient cases.

The measured streamwise variation of the local maximum velocity defect for the zero, favorable, and adverse pressure gradient cases is presented in Fig. 7. The maximum defect for the zero pressure gradient case exhibits the expected $x^{-1/2}$ variation commencing near $x/\theta_0 \approx 70$. The velocity defect decay is significantly reduced by imposition of the adverse pressure gradient. In fact, it may be noted that for the APG case the velocity defect actually grows slightly for $x/\theta_0 > 125$. In contrast, for the FPG and SFPG cases the velocity defect decays much more rapidly than for the ZPG case.

Note that in both Figs. 6 and 7 the response of the mean flow to the imposed pressure gradient is very rapid with both δ and U_d showing deviations from the zero pressure gradient case just downstream of location x_p.

Figure 8 presents measured wake half-width δ and maxi-

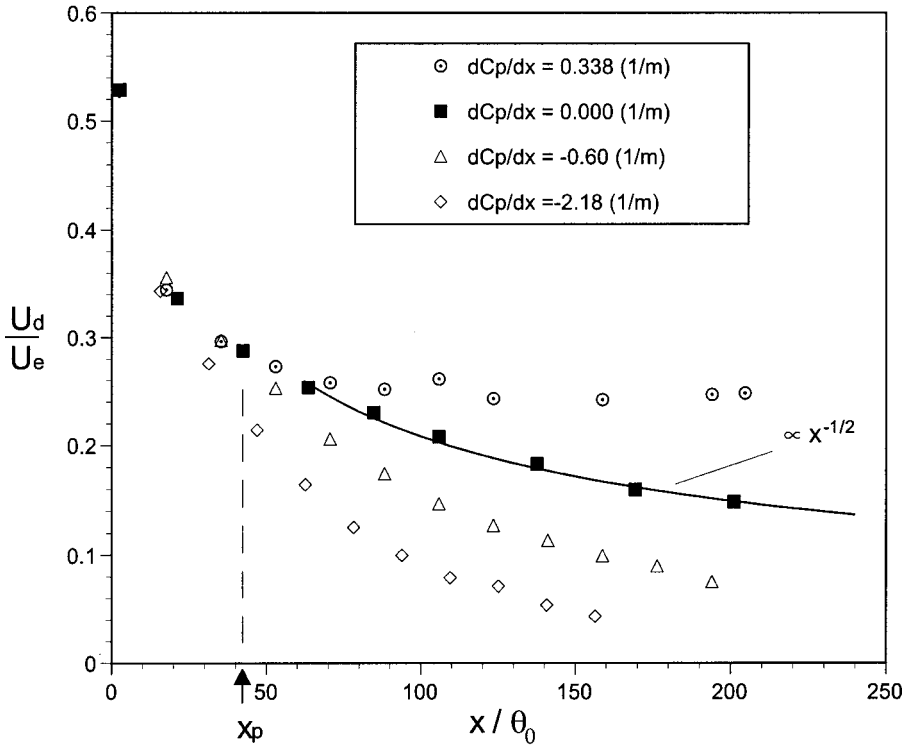

FIG. 7. Streamwise variation of the maximum velocity defect for different pressure gradient cases.

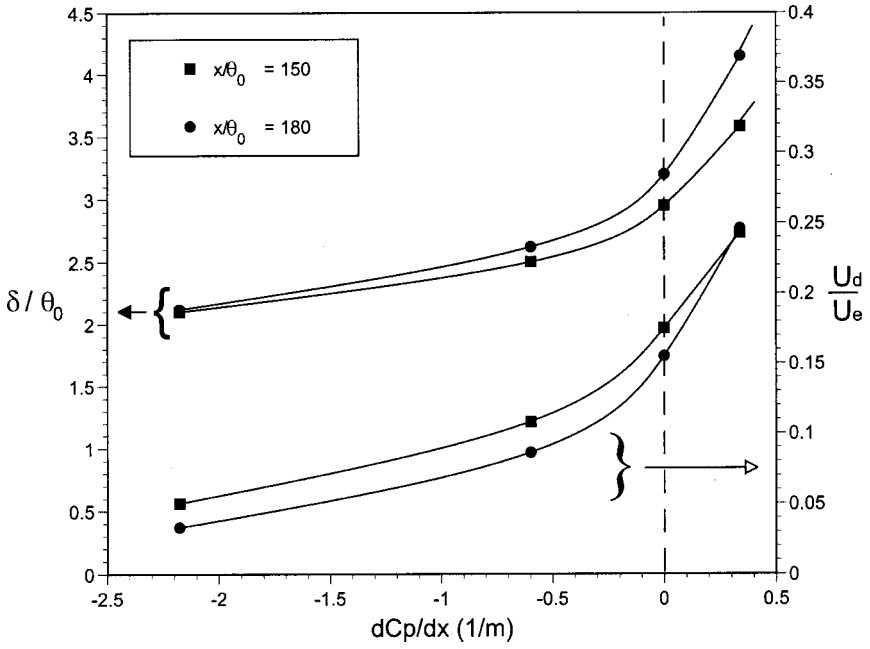

FIG. 8. Influence of imposed constant pressure gradient on wake half-width and maximum velocity defect at representative streamwise locations.

mum defect U_d at two representative streamwise locations in the diffuser as a function of the imposed constant pressure gradient. It is clear from Fig. 8 that the sensitivity of the wake mean flow to the imposed pressure field is not symmetric with respect to the zero pressure gradient condition. Rather, Fig. 8 shows that the wake's mean flow response is considerably more sensitive to adverse pressure gradients.

Figure 9 compares measured wake mean velocity profiles in ZPG, APG, FPG, and SFPG conditions at selected representative streamwise locations. The local velocity defect is scaled by $U_d(x)$ while the lateral spatial coordinate is scaled with $\delta(x)$. Using this scaling, it is apparent that the wake mean velocity profiles exhibit similarity and are nearly universal in shape despite the very different imposed pressure gradients. In each case the measurements in Fig. 9 conform quite well to the profile of form

$$\frac{U_e-\overline{U}}{U_d}=\exp(-0.637(y/\delta)^2-0.056(y/\delta)^4), \tag{1}$$

which is identical to that used by Wygnanski *et al.*[23] to collapse wake profiles generated by several different screens,

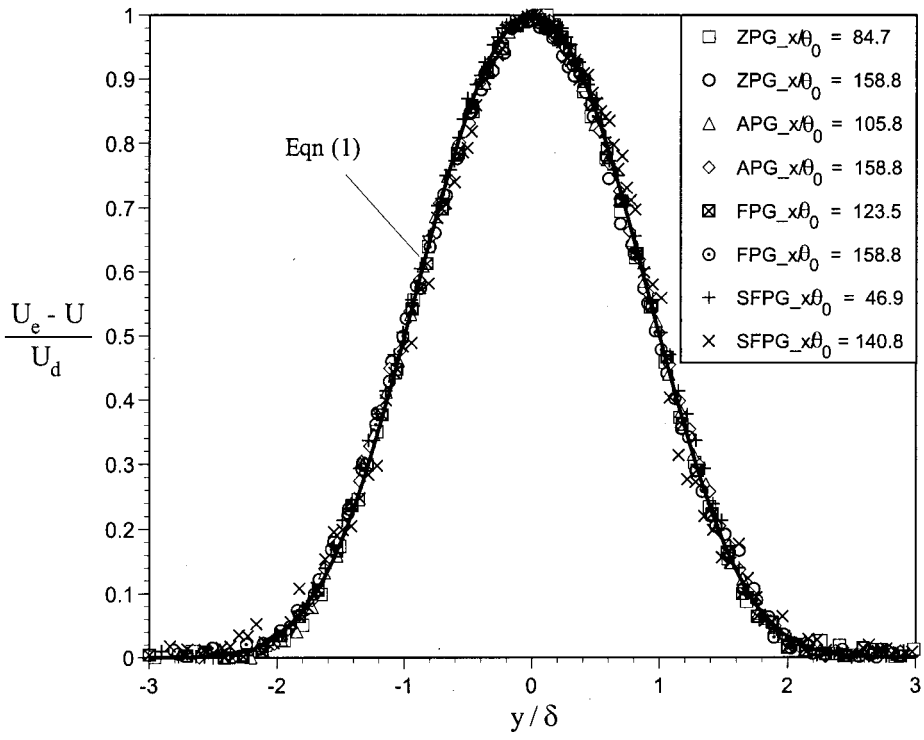

FIG. 9. Similarity of measured wake mean velocity profile shape for different pressure gradients.

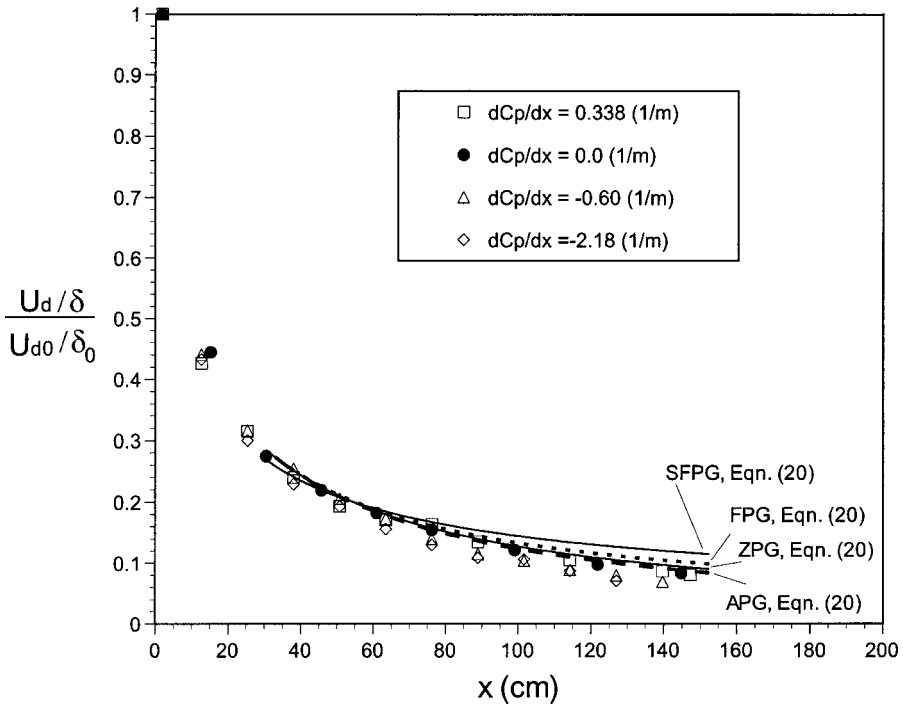

FIG. 10. Streamwise variation of U_d/δ for different pressure gradient cases.

cylinders, and airfoil shapes under zero pressure gradient conditions. Rogers[19] also reports a nearly universal profile shape for DNS simulations of a planar turbulent wake involving constant positive and negative imposed streamwise strain rates. It is also interesting to note that in an actual high-lift flow field, the outermost wake-like portion of the main element confluent boundary layer exhibited self-similarity despite the strong adverse pressure gradient environment as reported by Thomas *et al.*[24] It should also be pointed out, however, that profiles of normal and Reynolds stresses corresponding to the cases shown in Fig. 9 *do not* generally exhibit similarity when scaled appropriately by δ and U_d. In this sense the similarity encountered in these experiments is incomplete. This is certainly not surprising. It is well known that mean velocity similarity in free shear flows typically occurs upstream of the onset of similarity for the second-order turbulent statistics. In fact, despite collapse of the mean velocity profiles, the results of Wygnanski *et al.*[23] demonstrated a substantial dependence of wake initial conditions even far downstream of the wake generating body. For example, different spreading rates were measured for different wake-generating bodies although the wake mean velocity profiles appeared to be self-preserving in each case. This suggests that the turbulent wake may never reach a self-preserving state that is completely independent of initial conditions. Based on this, George[25] suggested a less restrictive interpretation of self-preservation for free shear flows and presents an analysis which allows for a multiplicity of self-preserving states. His analysis suggests that for a given free shear flow, the self-preserving state that is actually observed will depend upon initial conditions.

The wakes investigated in this study share a common origin but are exposed to very different pressure gradients for $x > x_p$. Consequently, at a given streamwise measurement station the upstream history of these wake flows will be quite different. Despite this, wake mean velocity profiles shown in Fig. 9 exhibit a remarkable collapse. It is of interest to examine the conditions under which the observed universal mean velocity profile shape occurs and, perhaps more importantly, whether this limited degree of similarity can be exploited in order to predict the wake spreading and defect decay for arbitrary pressure gradients. This is the topic to which we will turn our attention in Sec. V.

Figure 10 presents the streamwise evolution of the ratio U_d/δ as measured for each of the pressure gradient cases. This quantity is directly proportional to the absolute value of the maximum local mean strain rate $|\partial U/\partial y|_{\max}$. In particular, for the profile $f(y/\delta)$ shown in Fig. 9, the local maximum strain rate $|\partial U/\partial y|_{\max} = (U_d/\delta)|f'|_{\max}$. The normalized ordinate used in Fig. 10 accounts for the fact that the initial value U_{d0}/δ_0 for the SFPG case is different than for the other three cases since that experiment was performed at a lower Reynolds number. The measured streamwise evolution of U_d/δ shown in Fig. 10 is consistent with a reduction in maximum mean strain rate with streamwise distance. Note, however, that the streamwise variation of U_d/δ is virtually identical for each pressure gradient case. This may seem surprising given the very significant differences in the measured streamwise evolution of $\delta(x)$ and $U_d(x)$ shown in Figs. 6 and 7, respectively. In order to understand this note that, to good approximation, the mean spanwise vorticity $\overline{\Omega}_z \approx -\frac{1}{2}\partial\overline{U}/\partial y$. Upstream of imposition of the pressure gradient the mean spanwise vorticity is identical in each case, consistent with maintenance of the same initial conditions [see Fig. 5(a)]. The Reynolds-averaged vorticity transport equation shows that the redistribution of spanwise vorticity will be independent of the direct effects of the imposed pressure gradient ($\nabla \times \nabla P = 0$). Physically, this is a consequence of the fact that pressure forces act through the centroid of fluid

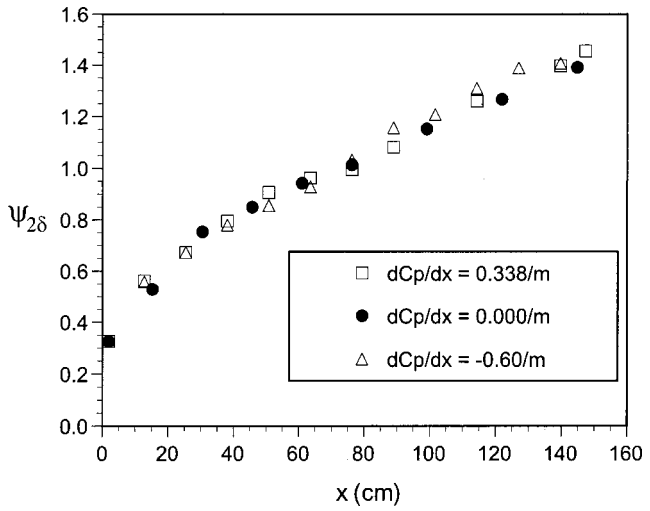

FIG. 11. Streamwise variation of mean streamfunction ψ corresponding to the lateral position $\eta=2$.

elements. Consequently, the imposed pressure gradient will manifest itself only indirectly through its effect on the turbulent field (as described in Sec. IV B) and consequently, on spatial gradients of correlations between fluctuating velocity and fluctuating vorticity.

At each streamwise location, x, the streamfunction corresponding to a particular cross-stream distance from the wake centerline can be computed. Using the self-similar wake mean velocity profiles shown in Fig. 9, and assuming that the value of the streamfunction on the wake centerline is $\psi=0$, (i.e., symmetric wake) we obtain

$$\psi=U_e\delta\left[\eta-\frac{U_d}{U_e}\int_0^{\eta}f(\eta')d\eta'\right], \tag{2}$$

where $\eta\equiv y/\delta(x)$. As an example, Fig. 11 presents the streamwise variation in the mean streamfunction ψ corresponding to the arbitrary lateral position $\eta=2$ as obtained at selected streamwise locations. The ZPG, FPG, and APG cases are shown in Fig. 11. The SFPG case has been excluded since that experiment was run at a different Reynolds number (and hence, volumetric flow rate). Figure 11 shows that, to good approximation, all cases collapse to exhibit a common streamwise variation. This was found to be true regardless of the lateral extent over which the integration was performed. Since the diffuser wall is, to good approximation, a mean streamline for the flow, and since each of the experiments shown was performed at the same flow rate, this presentation of wake evolution in $\psi-x$ space maps the diffuser wall to a common locus $\psi=$ const. That the streamwise evolution of ψ associated with a given lateral position in the wake is common across all pressure gradient cases is indicative that the mechanism by which the wake mean flow responds to the imposed pressure gradient is common to all cases. That is, the growth rate of the wake in $\psi-x$ space is independent of the imposed pressure gradient. In addition, since the ψ value corresponding to fixed η is *not* constant, it also shows that the wake boundary does not simply follow the imposed external inviscid streamlines. The streamwise increase in the value of ψ corresponding to a fixed η is a result of the lateral propagation of the edge of the wake into the inviscid flow region and the mechanism for this propagation is mainly due to turbulent diffusion. It is to the characterization of the second-order turbulence statistics that we turn our attention in the following.

B. Wake turbulence quantities

The imposed pressure gradients also have a pronounced effect on turbulence quantities measured in the wake. Perhaps the most fundamental and physically descriptive of these is the turbulent kinetic energy per unit mass, $k=\frac{1}{2}(\overline{u'^2}+\overline{v'^2}+\overline{w'^2})$. Using X-wire measurements, profiles of the required normal stresses were measured at selected streamwise locations and the local turbulent kinetic energy computed. Figure 12 presents shaded iso-contours of the wake turbulent kinetic energy in the $x-y$ plane for APG, ZPG, FPG, and SFPG conditions. Note that the lateral coordinate y has been left unscaled in order that the associated effect of pressure gradient on the wake spreading may also be observed. Upstream of x_p the turbulent kinetic energy distributions are virtually identical with the exception of the SFPG case which was run at a somewhat lower Reynolds number. Figure 12 shows that along with the enhanced lateral wake growth, the adverse pressure gradient condition sustains higher levels of turbulent kinetic energy over larger streamwise distances than in the zero pressure gradient wake. In contrast, the favorable pressure gradient cases exhibit a more rapid decay of turbulence kinetic energy relative to the zero pressure gradient case.

Figure 13 presents cross-stream profiles of $\sqrt{\overline{u'^2}}/U_d$ measured via LDV at several representative streamwise locations for each of the pressure gradient cases. Figure 13 illustrates another key difference which involves the rate at which the profiles of second-order turbulent statistics approach self-similarity. In the case of the adverse pressure gradient, the tendency for the scaled rms profiles to approach collapse is apparent and is clearly accelerated over and above that exhibited by the ZPG case. In marked contrast, the FPG and SFPG cases show little evidence of an approach to self-similar behavior.

As one might well expect, the trends shown in Fig. 13 are not exclusive to the streamwise fluctuating velocity component. Figure 14 presents the streamwise evolution of $\sqrt{\overline{u'^2}}/U_d$, $\sqrt{\overline{v'^2}}/U_d$, and $\overline{u'v'}/U_d^2$ as measured at the arbitrary lateral location $y=0.8\delta$. For each scaled statistical quantity, the accelerated approach of the turbulence to similarity for the APG case is apparent while the FPG and SFPG cases show no evidence of approaching an asymptotic value. Note that the turbulent statistics for the ZPG case are just beginning to approach a limiting value near the downstream end of the diffuser test section.

Figure 15 presents cross-stream profiles of the Reynolds stress normalized by the local turbulent kinetic energy as measured at several representative streamwise locations for the APG, FPG, and SFPG cases. It is apparent from Fig. 15 that in each case the Reynolds stress profiles exhibit a reasonable collapse when scaled by k. That $\overline{u'v'}$ scales with k

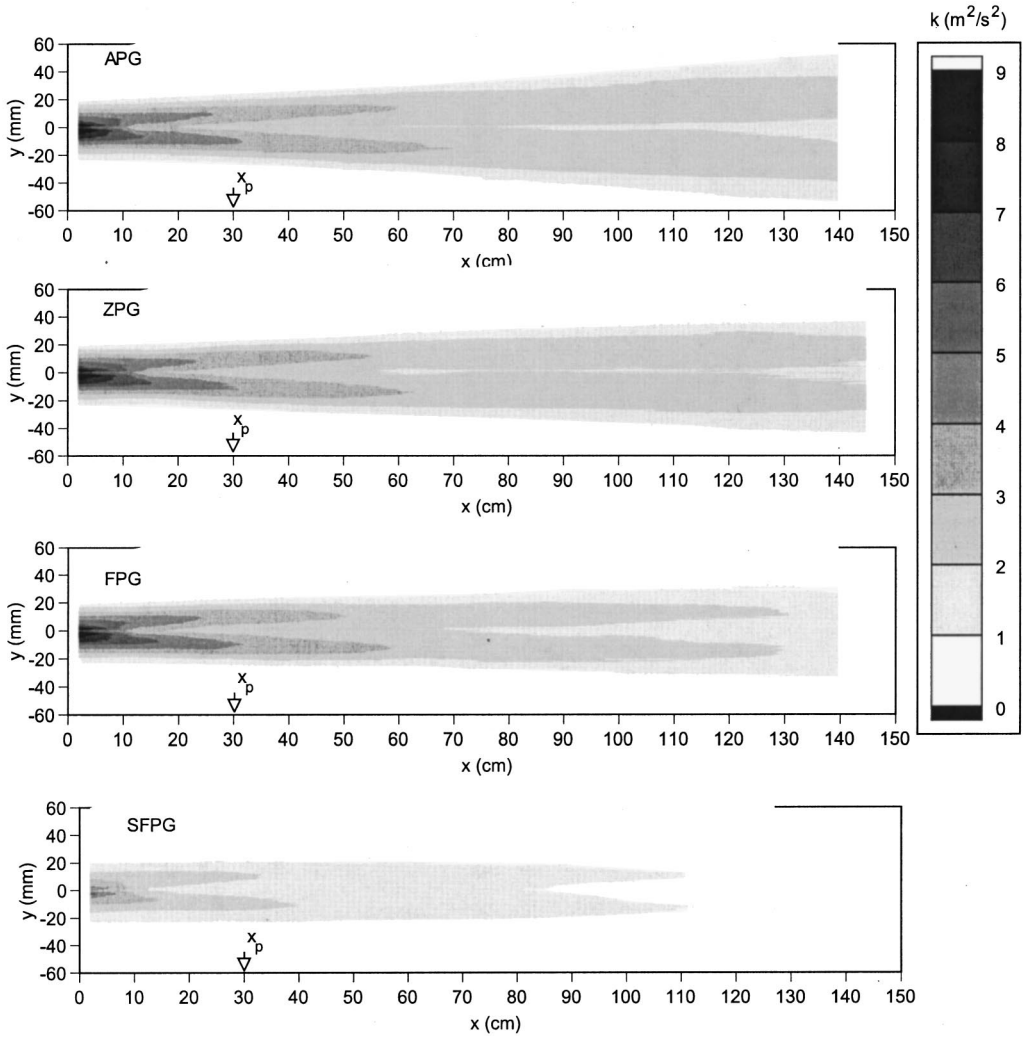

FIG. 12. Turbulent kinetic energy iso-contours for the APG, ZPG, FPG, and SFPG cases.

has important implications regarding the applicability of algebraic Reynolds stress closure models to this class of strained flows. Inherent to the algebraic stress model originally proposed by Rodi is the so-called weak-equilibrium assumption,[26]

$$\frac{\overline{D}}{\overline{D}_t}(\overline{u_i' u_j'}) \approx \frac{\overline{u_i' u_j'}}{k}\frac{\overline{D}k}{\overline{D}t}, \tag{3}$$

which is equivalent to assuming that $(\overline{D}/\overline{D}t)(\overline{u_i' u_j'}/k)=0$. For the wake flow under investigation here, it is clear from Fig. 15 that if the lateral coordinate is scaled by δ, then $(\partial/\partial x)(\overline{u'v'}/k)=0$ for both favorable and adverse gradients. Measurements confirm that $\overline{V}(\partial/\partial y)(\overline{u'v'}/k)$ is generally quite small across the wake as well. These results suggest that the neglect of variations of $\overline{u'v'}$ that are due to the anisotropy tensor while retaining those due to k is a very reasonable approximation for this strained turbulent wake flow.

In the similarity analysis which appears in Sec. V, the x dependence of the scaled Reynolds stress, $-\overline{u'v'}/U_d^2$, is accounted for by an amplitude function $G_{uv}(x) \equiv \overline{u'v'}_{\max}/U_d^2$ which acts on a supposedly universal lateral shape function $g(\eta)$. Figure 16 presents the measured profiles of $g(\eta)$ obtained throughout the diffuser section corresponding to the APG, ZPG, FPG, and SFPG cases. Figure 16 clearly shows that the shape function $g(\eta)$ is indeed independent of the applied pressure gradient. Also shown for comparison is the function $g(\eta)$ resulting from integration of Eq. (13). The agreement with the measured profile shapes is reasonable. Figure 16 indicates that the imposed pressure gradient has no effect on the cross-stream shape of the Reynolds stress profiles although it certainly does influence $G_{uv}(x)$ as suggested by Fig. 14.

One may question whether the scaled normal turbulent stresses exhibit a cross-stream profile shape that is independent of the imposed pressure gradient condition. Figure 17 presents profiles of $h(\eta) \equiv \overline{u'^2}/(G_{uu}(x)U_d^2)$ (where $G_{uu}(x) \equiv \overline{u'^2}_{\max}/U_d^2$ for each pressure gradient case). Figure 17 shows that, unlike the Reynolds stresses, the normal stresses do not exhibit a cross-stream shape that is independent of either streamwise coordinate or imposed pressure gradient. Some insight regarding this behavior may be gained by noting that in each case the profiles are most dissimilar near the

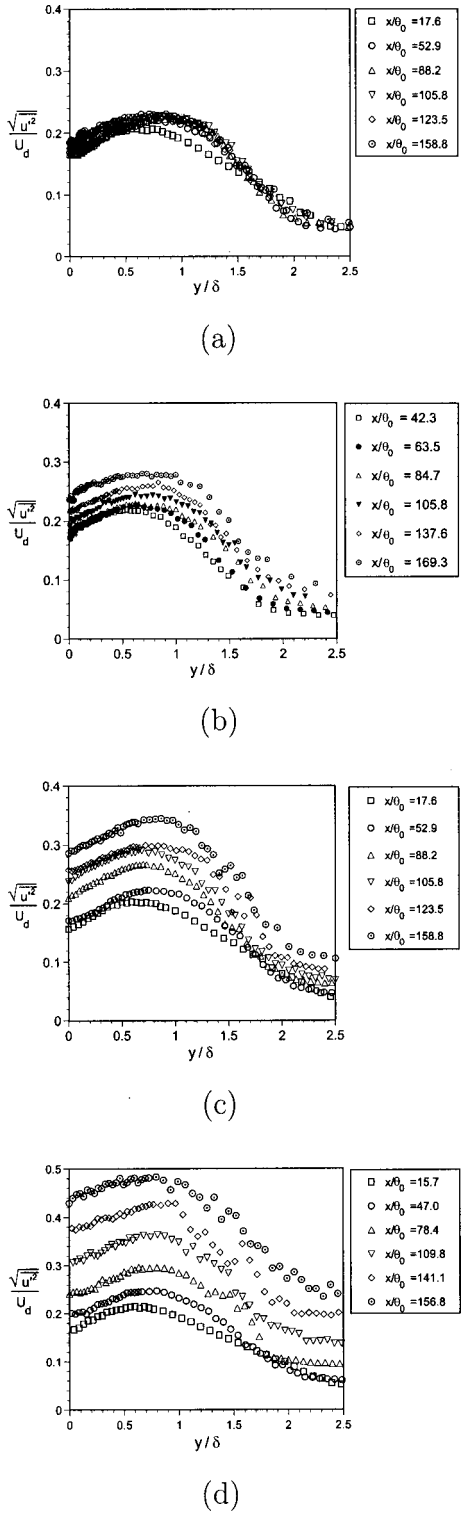

FIG. 13. Representative cross-stream profiles of $\sqrt{\overline{u'^2}}/U_d$ for different pressure gradient cases. (a) APG; (b) ZPG; (c) FPG; (d) SFPG.

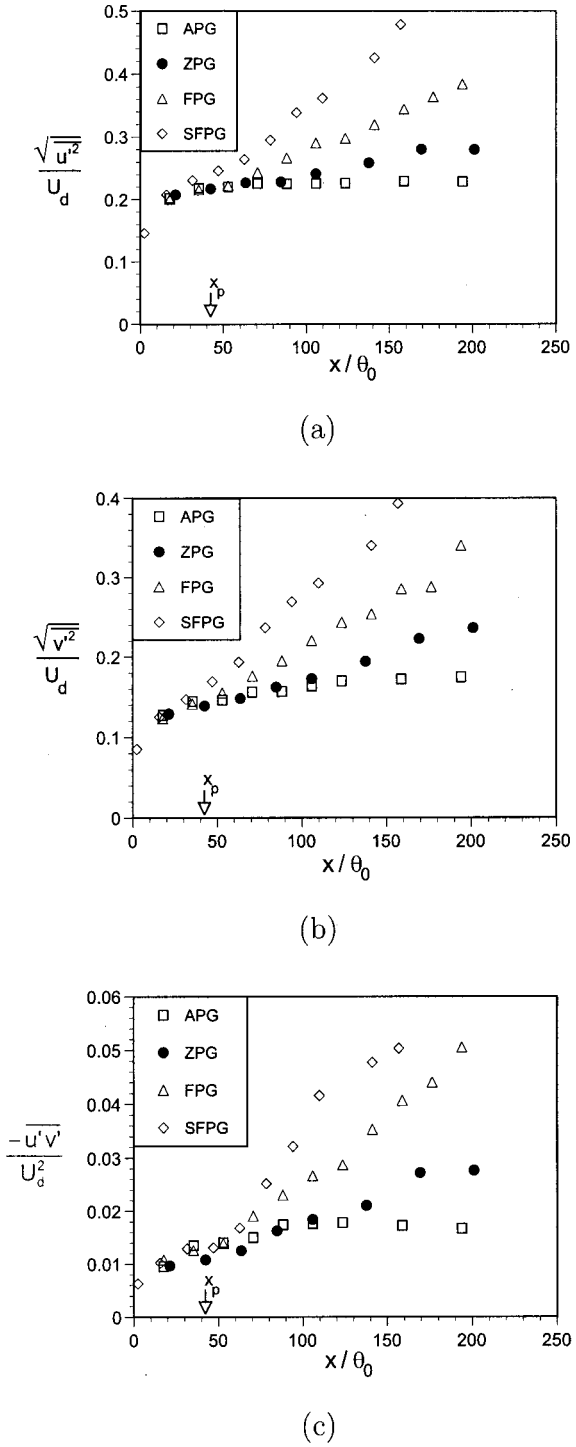

FIG. 14. Streamwise evolution of normal and Reynolds stresses at $y/\delta = 0.8$ for the APG, ZPG, FPG, and SFPG cases. (a) Streamwise component normal stress $\sqrt{\overline{u'^2}}$; (b) lateral component normal stress $\sqrt{\overline{v'^2}}$; (c) Reynolds stress $-\overline{u'v'}$.

centerline of wake. Since turbulence production is zero there, the turbulence on the centerline is due to transport by advection and/or turbulent diffusion. Consequently, similarity of the normal stress profiles requires a higher level self-similar behavior than that required for the Reynolds stresses. More specifically, it requires similarity at the level of the turbulent kinetic energy transport equation. Although not presented in this paper, Liu[27] measured the full turbulent kinetic energy budget for the APG, ZPG, and FPG cases. Scaling issues related to the various terms were explored and, consistent with the results shown in Fig. 17, significant differences in the turbulent advection terms were noted between the different cases.

In these experiments turbulence production can occur

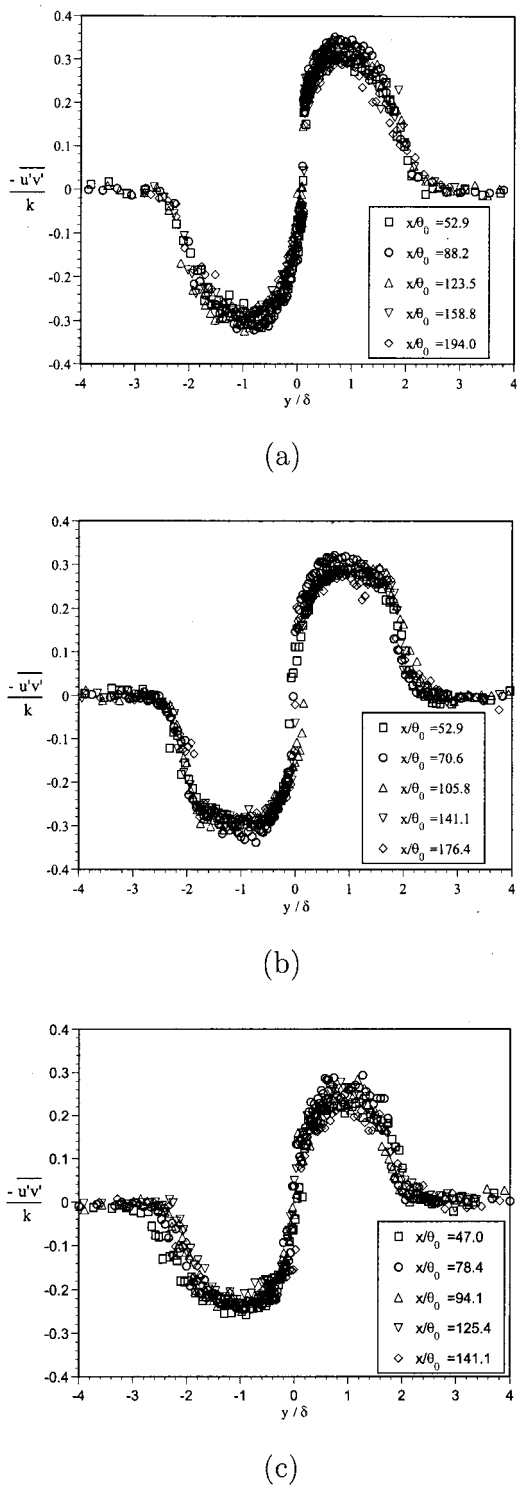

FIG. 15. Cross-stream profiles of the Reynolds stress normalized by the local turbulent kinetic energy at several representative streamwise locations for the APG, FPG, and SFPG cases. (a) APG case; (b) FPG case; (c) SFPG case.

not only by the local shear production terms, $-\overline{u'v'}\,\partial\overline{U}/\partial y$ and $-\overline{u'v'}\,\partial\overline{V}/\partial x$, but also by the dilatational production term, $-(\overline{u'^2}-\overline{v'^2})\,\partial\overline{U}/\partial x$. Since $\overline{u'^2}>\overline{v'^2}$, the latter term is positive for the adverse pressure gradient case and represents an additional source for turbulence. For the favorable pressure gradient cases, the term is negative and represents the transfer of turbulent kinetic energy back to the mean flow. Although not presented here, the shear production term, $-\overline{u'v'}\,\partial\overline{V}/\partial x$, was measured and found to be entirely negligible. In order to assess the relative significance of the remaining production terms, profiles of each were measured at selected streamwise locations throughout the wake for each pressure gradient case. As an example, Fig. 18 compares the local shear production term $-\overline{u'v'}\,\partial\overline{U}/\partial y$ with the dilatational production term $-(\overline{u'^2}-\overline{v'^2})\,\partial\overline{U}/\partial x$ as measured at $x/\theta_0=106$ for each of the pressure gradient conditions. In each case the production term has been scaled by the common factor θ_0/U_{e0}^3. From Fig. 18, it can be seen that the flow is clearly shear dominated despite the imposed pressure gradients. Even for the SFPG case, the magnitude of shear production term is greater than that of the dilatational term. This is not to say that the effect of the dilatational term on the flow is without significance. Note that the dilatational term serves to augment the turbulence for the APG case and significantly reduces the turbulence production for the two favorable pressure gradient cases shown.

The streamwise development of the scaled turbulence production as measured at $y/\delta=0.95$ (the location of maximum local $\partial\overline{U}/\partial y$) is presented in Fig. 19 for each of the pressure gradient conditions. In each case the turbulence production decreases with streamwise distance. This reduction in turbulence production is expected given the streamwise variation in U_d/δ (a quantity intimately related to the maximum mean strain rate) shown in Fig. 10. However, unlike $\partial\overline{U}/\partial y$, the streamwise decay in turbulence production varies significantly with imposed pressure gradient. It is greatest for the favorable pressure gradient cases and this apparently gives rise to the more rapid streamwise decay in k shown previously in Fig. 12. In contrast, Fig. 19 shows that for the APG case the local turbulence production exceeds that of the ZPG case at each streamwise location giving rise to the higher sustained k values shown in Fig. 12. Since the streamwise variation in the mean strain rate $\partial\overline{U}/\partial y$ is common to each of the cases, the differences shown in Fig. 19 must originate with the Reynolds stress $-\overline{u'v'}$ and/or the dilatational production term.

Figure 20 compares measured cross-stream profiles of $-\overline{u'v'}$ for the FPG and APG cases at four representative streamwise locations downstream of imposition of the pressure gradient. Initially, the profiles are identical but with increased streamwise distance the APG case exhibits larger values. In order to assess whether the imposed pressure gradient had an effect on the phase relationship between the u' and v' fluctuations, the streamwise evolution of the Reynolds stress correlation coefficient function $\rho_{uv}=\overline{u'v'}/\sqrt{\overline{u'^2}}\sqrt{\overline{v'^2}}$ was examined for each pressure gradient case. Although not presented here, the correlation coefficient was quite similar for each of the cases and exhibited little variation with streamwise distance with nominal local maximum values of $\rho_{uv}\approx 0.42$. This suggests that the difference between the cases shown in Fig. 20 is associated primarily with the amplitude of the fluctuations rather than their phase relationship.

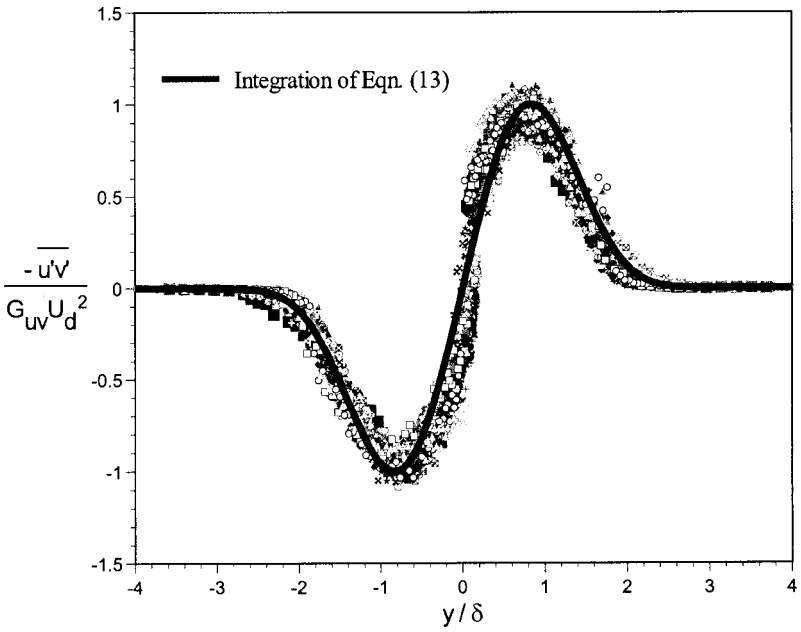

FIG. 16. Summary of all measurements of the wake Reynolds stress shape function $g(\eta)$ for APG, ZPG, FPG, and SFPG cases taken throughout the diffuser test section.

In an effort to assess the relative importance of the dilatational and shear production terms in accounting for the differences between cases shown in Fig. 19, we define Δ to be the local difference between turbulence production for the APG and FPG cases. This difference is composed of contributions associated with the difference in the dilatational terms Δ_d and shear production terms Δ_s. Figure 21 presents the measured streamwise variation of the ratios Δ_d/Δ and Δ_s/Δ (expressed as a percentage). Near the location where the pressure gradient is first imposed $\Delta_d/\Delta \approx 100\%$ since the response of the mean flow to the streamwise straining $\partial\overline{U}/\partial x$ is immediate while the Reynolds stresses are more slow to respond, as shown in Fig. 20. As they do, the ratio Δ_s/Δ grows to account for approximately 80% of Δ. In other words, with increasing distance downstream the effect of the dilatational term in augmenting fluctuations for the APG case and suppressing them for the FPG case leads to the disparity in $-\overline{u'v'}$ shown in Fig. 20. The increasing disparity between the shear production terms with streamwise distance is reflected by the rise of the Δ_s/Δ. In this manner the dilatational production term initially triggers the differences in k between the FPG and APG cases. The associated disparity in $-\overline{u'v'}$ between cases gives rise to the differing rates of shear production shown in Fig. 19.

V. WAKE MEAN FLOW SIMILARITY CONSIDERATIONS

The governing equations for the wake flow are the thin shear layer form of the momentum equation,

$$\overline{U}\frac{\partial\overline{U}}{\partial x}+\overline{V}\frac{\partial\overline{U}}{\partial y}=U_e\frac{dU_e}{dx}-\frac{\partial(\overline{u'v'})}{\partial y} \tag{4}$$

and mass conservation,

$$\frac{\partial\overline{U}}{\partial x}+\frac{\partial\overline{V}}{\partial y}=0, \tag{5}$$

where primes denote fluctuating quantities and overbars indicate time averaging. Note that the viscous stress term has not been included. Neglect of the viscous term is based on recognition that the characteristic time scale for viscous diffusion of momentum $t_{\text{visc}}\sim O(\delta^2/\nu)$ is much greater than both the characteristic residence time of fluid particles in the diffuser test section $t_{\text{res}}\sim O(L/U_e)$ and the characteristic time scale for turbulent momentum transfer $t_{\text{turb}}\sim O(\delta/u')$. Here L denotes the streamwise extent of the diffuser test section and u' is a representative measure of the fluctuating velocity. The requirement that $t_{\text{visc}}\gg t_{\text{turb}}$ is equivalent to requiring that $\text{Re}_t\equiv u'\delta/\nu\gg 1$. That is, the turbulent Reynolds number must be large. Calculations verify that for the experiments reported here $u'\delta/\nu\sim O(10^3)$, where u' is taken as the rms streamwise velocity. This indicates that turbulent momentum transport is three orders of magnitude larger than viscous transport. Similarly, requiring $t_{\text{visc}}\gg t_{\text{res}}$ is equivalent to $(L/\delta)\ (\nu/U_e\delta)\ll 1$. For these experiments calculations show that $(L/\delta)(\nu/U_e\delta)\sim O(10^{-3})$, indicating that the residence time in the diffuser is simply too short for viscous transport to be significant.

Defining the following similarity variables,

$$f(\eta)\equiv\frac{U_e-\overline{U}}{U_d},\quad G_{uv}(x)g(\eta)\equiv\frac{-\overline{u'v'}}{U_d^2},\quad \eta\equiv\frac{y}{\delta(x)},$$

where it is noted that the scaled Reynolds stress is taken as the product of an x-dependent amplitude function $G_{uv}(x)$ and a lateral shape function $g(\eta)$. This scaling is appropriate for the near-wake under consideration here. In fact, similar scaling has been suggested by George[25] as the preferred form for asymptotic free shear layer evolution in order to properly account for initial conditions. Substituting into (4), and using (5) yields

$$Af+Bf^2+C\eta f'+Df'\int_0^\eta f\,d\eta=G_{uv}(x)g', \tag{6}$$

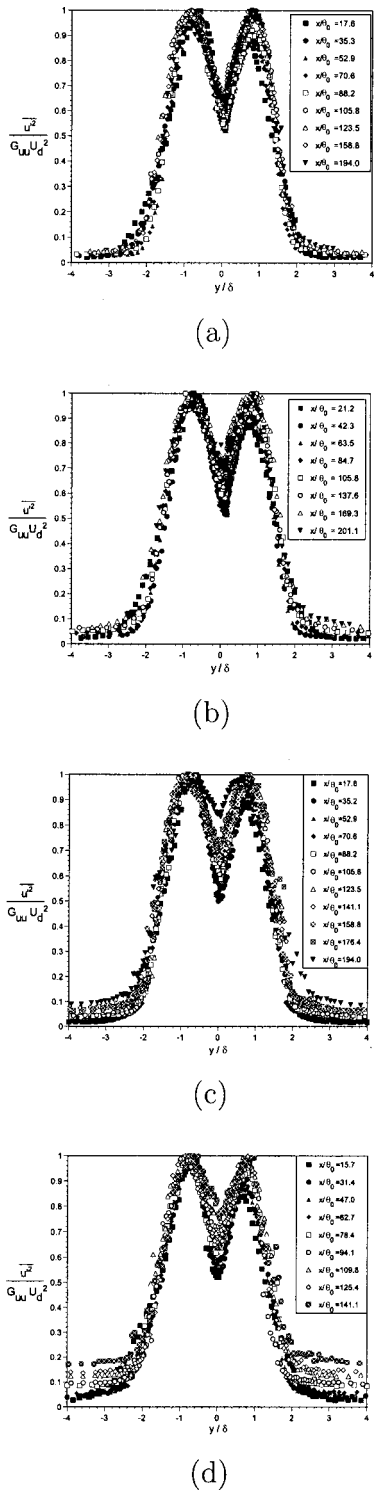

FIG. 17. The normal stress shape function $h(\eta)$ at different streamwise locations. (a) APG; (b) ZPG; (c) FPG; (d) SFPG.

where primes denote differentiation with respect to η and the coefficients on the left-hand side are given by

$$A=-\left[\frac{\delta}{U_d^2}\frac{d(U_eU_d)}{dx}\right],\quad B=\left[\frac{\delta}{U_d}\frac{dU_d}{dx}\right],$$
$$C=\left[\frac{1}{U_d}\frac{d(U_e\delta)}{dx}\right],\quad D=-\left[\frac{1}{U_d}\frac{d(U_d\delta)}{dx}\right]. \tag{7}$$

In order for similarity to occur, the coefficients A, B, C, D, and G_{uv} must remain proportional to each other as the flow evolves in x. Cross-stream integration of (6) shows that

$$A-C=\beta(D-B), \tag{8}$$

where $\beta\equiv(\int_{-\infty}^{+\infty}f^2\,d\eta)/(\int_{-\infty}^{+\infty}f\,d\eta)=0.73$ for the profile given by (1). Examination of (6) and (7) shows that similarity can only be achieved under the rather restrictive assumption that U_e is proportional to U_d. If we suppose that $U_e=\alpha U_d$ then it follows that $A=-2\alpha B$ and $C=-\alpha D$. Using relation (8) we also have $D=B(2\alpha-\beta)/(\alpha-\beta)$. Thus for self-similarity, relation (6) becomes

$$-2\alpha f+f^2-\alpha\frac{(2\alpha-\beta)}{(\alpha-\beta)}\eta f'+\frac{(2\alpha-\beta)}{(\alpha-\beta)}f'\int_0^\eta f\,d\eta$$
$$=\frac{G_{uv}(x)}{B(x)}g', \tag{9}$$

which shows that similarity also requires that $G_{uv}(x)$ be proportional to $B(x)$.

Let us first consider the implications for the APG case. Figure 7 shows that, to good approximation, $U_e\approx\alpha U_d$ with $\alpha\approx4$. Taking $\beta=0.73$ we find that $A\approx-8B$, $C\approx-8.89B$, and $D\approx2.22B$. From this we see that B and D are small compared to A and C and that $A\approx0.9C$. Now from Fig. 14(c) it is also found that for the APG case, $G_{uv}(x)$ is constant and therefore so too is B according to the similarity requirement.

We next consider the FPG case. In this case the coefficients A, B, C, and D cannot be proportional since the velocity defect is clearly not proportional to the external velocity, as shown in Fig. 7. However, Fig. 6 does show that for the SFPG case δ is constant (parallel flow) and even in the FPG case it appears that this condition is gradually approached near the end of the diffuser test section. Taking $d\delta/dx=0$ and defining $Q\equiv(U_e/2U_d)$ we find that $A=-B(\beta+Q)$, $B=B$, $C=B(\beta-Q)$, and $D=-B$. From Fig. 7 it is apparent that Q continually increases with streamwise distance and, in fact, is on the order of $O(10)$ near the end of the test section. With β fixed, it is apparent that the coefficients A and C will again dominate (6) with the dominance of these terms growing with streamwise distance x. Now $A-C=-2\beta B$ with the sign of B determined by $dU_d/dx<0$. Hence it follows that $A>C$ (which is opposite the APG case). Experiments show that for the FPG case, $C\approx0.8A$. Note, however, that for favorable pressure gradients, Q continues to increase as the flow evolves in x and the condition $A\approx C\approx-BQ$ is approached. This asymptotic condition yields a particularly simple relation for the velocity defect. In particular, for parallel flow with $\delta=\delta_0$, we obtain

$$\frac{U_d}{U_e}=\frac{U_{d0}U_{e0}^2}{U_e^3}. \tag{10}$$

Here the subscript 0 denotes initial values taken at the onset of the pressure gradient condition. Figure 22 compares the measured streamwise variation of U_d/U_e for the SFPG case with that predicted by relation (10). The agreement is observed to be quite good.

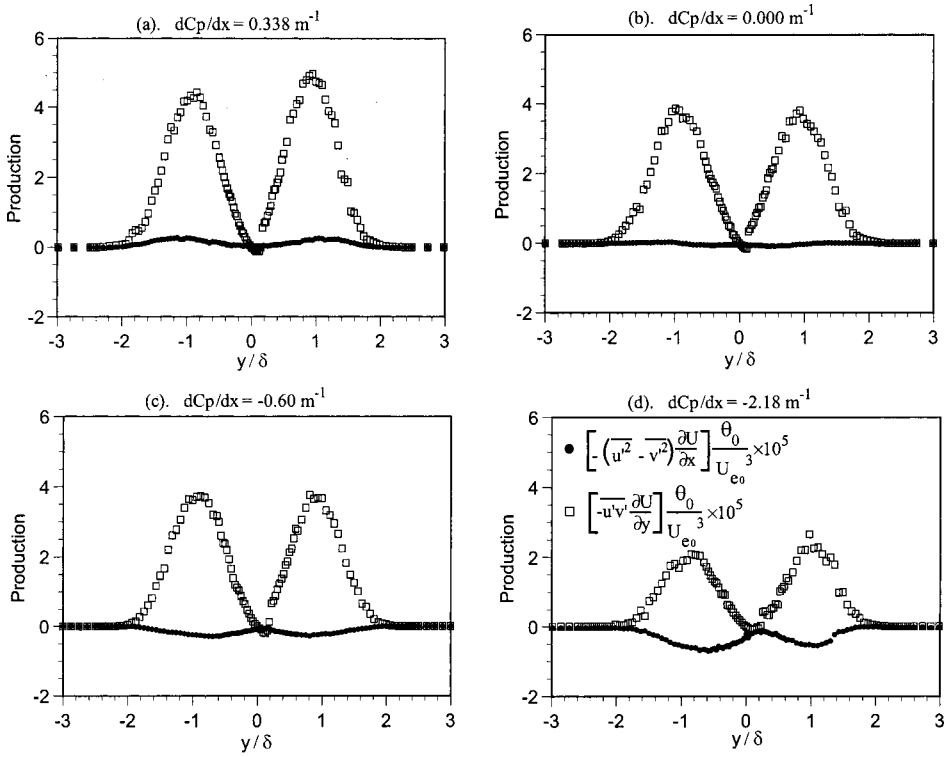

FIG. 18. Comparison of shear and dilatational turbulence production terms for different pressure gradients at $x/\theta_0=106$. (a) $dCp/dx=0.338\ \mathrm{m}^{-1}$; (b) $dCp/dx=0.0\ \mathrm{m}^{-1}$; (c) $dCp/dx=-0.60\ \mathrm{m}^{-1}$; (d) $dCp/dx=-2.18\ \mathrm{m}^{-1}$.

For both favorable and adverse pressure gradients cases we have shown that the coefficients A and C dominate (6) and that their size is comparable. If we make the approximation that

$$A \approx C \equiv K(x), \tag{11}$$

which, from (8), is equivalent to neglecting B and D, we obtain the approximate form of (6),

$$Af + C\eta f' = G_{uv} g' \tag{12}$$

or equivalently,

$$f + \eta f' = \frac{G_{uv}(x)}{K(x)} g'. \tag{13}$$

Relation (11) leads to the requirement that

$$U_e^{2n} U_d^n \delta^n = \text{const}, \tag{14}$$

where n is any number other than zero. Taking $n=1$, we define a grouping in (14) as

$$M \equiv U_e^2 U_d \delta = \text{const}. \tag{15}$$

Within the small velocity defect approximation, the above-mentioned grouping represents the wake mean flow kinetic energy defect flow rate which Eq. (15) states is constant. Measurements of the streamwise variation of M for each of the pressure gradient cases are presented in Fig. 23, where M_0 represents the initial M value in the wake. The value of M for the ZPG case is observed to be approximately constant with x. In contrast, M increases and decreases with x for the APG and FPG cases, respectively. This is a consequence of the previously documented imperfection of the assumption that $A=C$. Note, however, that Fig. 23 also indicates that the dependence of M on the streamwise coordinate is actually weak. If, corresponding to this observation, the approximation of Eq. (15) is retained, relation (11) may be solved to yield

$$\frac{(U_e\delta)^2}{M^2} = \frac{1}{(U_e U_d)^2} = \frac{2}{M}\int \frac{K}{U_e} dx + C_0, \tag{16}$$

where C_0 is a constant of integration. Equation (16) provides a means for predicting the streamwise variation of the global wake parameters $\delta(x)$ and $U_d(x)$ for a specified external

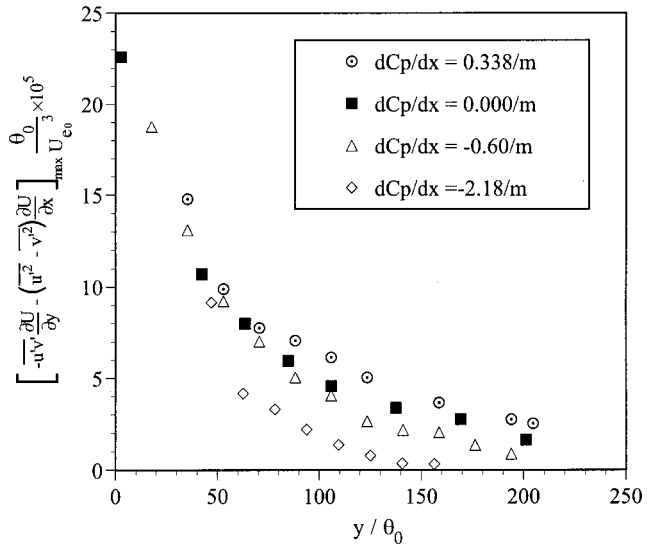

FIG. 19. Streamwise variation in turbulence production ($y/\delta=0.95$) for APG, ZPG, FPG, and SFPG cases.

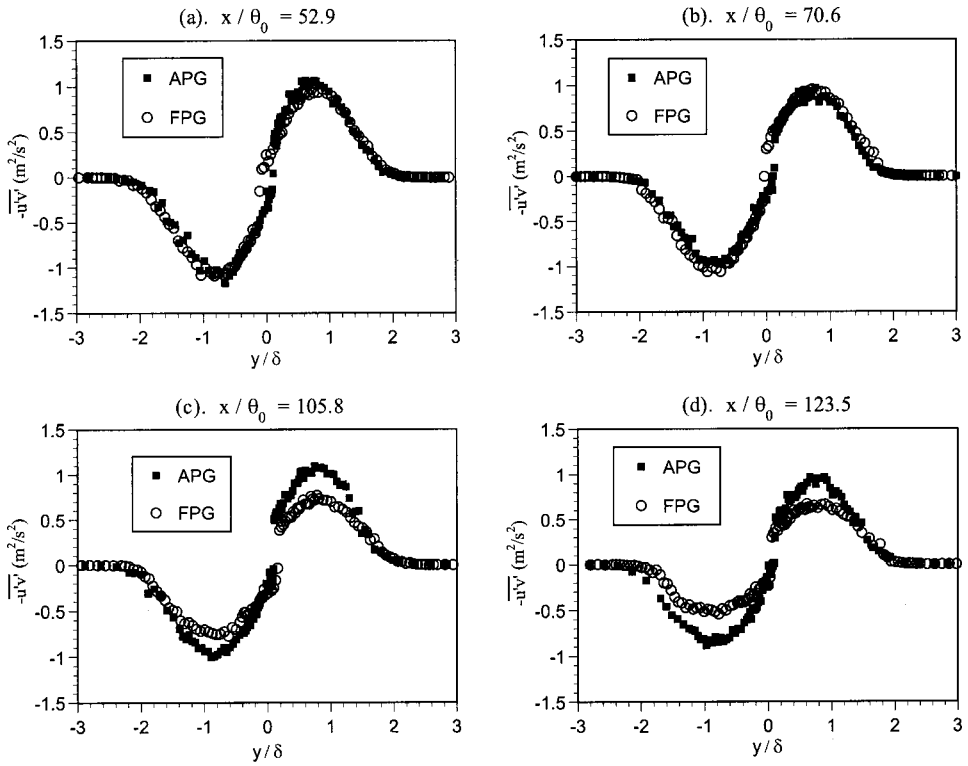

FIG. 20. Comparison of the $-\overline{u'v'}$ profiles at selected streamwise locations for APG and FPG cases. (a) $x/\theta_0=52.9$; (b) $x/\theta_0=70.6$; (c) $x/\theta_0=105.8$; (d) $x/\theta_0=123.5$.

velocity $U_e(x)$ (i.e., imposed pressure gradient). More specifically, solving (16) one obtains the following explicit expressions for $\delta(x)$ and $U_d(x)$:

$$\frac{\delta(x)}{\delta_0}=\frac{\sqrt{1+2(T^*-T_0^*)}}{U_e/U_{e0}}, \tag{17}$$

$$\frac{U_d(x)}{U_{d0}}=\frac{1}{(U_e/U_{e0})\sqrt{1+2(T^*-T_0^*)}}, \tag{18}$$

where the global wake parameters at the initial streamwise position $x=x_0$ are denoted δ_0 and U_{d0} and

$$T^*-T_0^*\equiv\frac{U_{d0}}{\delta_0}\int_{x_0}^{x}\frac{K(x)dx}{U_e(x)}. \tag{19}$$

Measurements of $K(x)$ by Liu[27] show that it exhibits only a weak streamwise dependence and we will approximate it as a constant. A suitable representation is $K\approx 0.044$ independent of the imposed pressure gradient. With K taken as a constant, relations (17) and (18) indicate that both global wake parameters $\delta(x)$ and $U_d(x)$ are only functions of the imposed external velocity $U_e(x)$. It may be noted that for the zero pressure gradient case (17) and (18) yield classic planar turbulent wake similarity scaling.

Figures 24 and 25 present comparisons of the streamwise variation of δ and U_d, respectively, as predicted from relations (17) and (18) with the experimental measurements

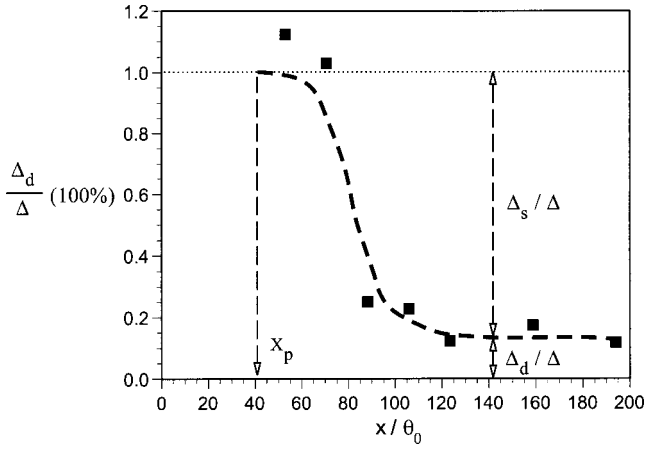

FIG. 21. Streamwise variation of the ratios Δ_d/Δ and Δ_s/Δ.

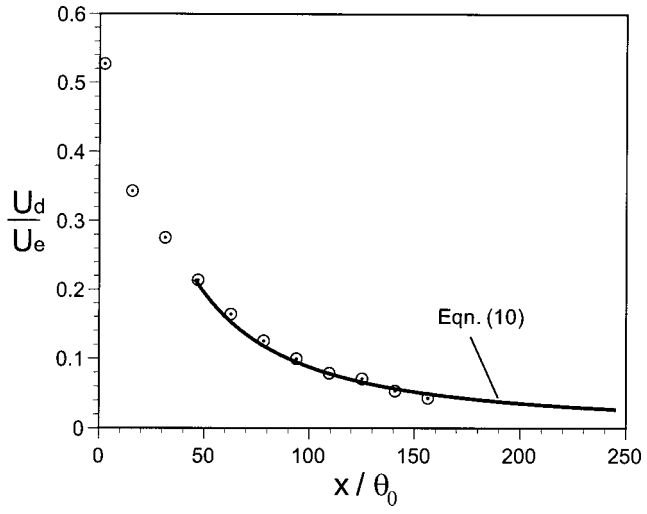

FIG. 22. Comparison of the measured streamwise variation of U_d/U_e for the SFPG case with the prediction by relation (10).

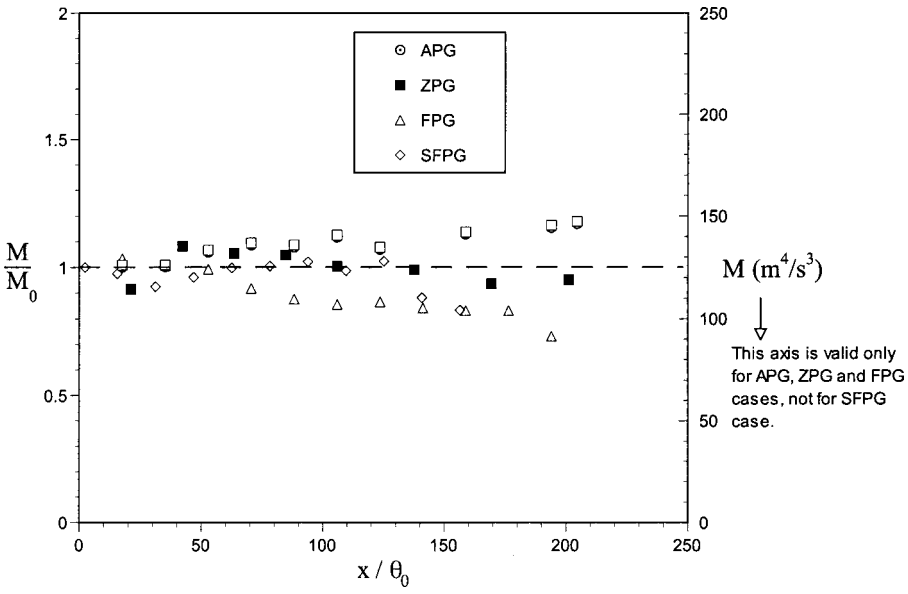

FIG. 23. Comparison of the streamwise variation of parameter M for APG, ZPG, FPG, and SFPG cases.

corresponding to the APG, ZPG, FPG and SFPG conditions. In each case the initial input position x_0 is taken as the location where the imposed pressure gradient commences. In most cases, the overall agreement is observed to be good with the analytical expressions capturing the essential aspects of the streamwise behavior of the wake mean flow parameters. For the velocity defect variation, the worst agreement is observed for the FPG case where (18) underpredicts the defect decay. It is interesting to note that the agreement is much better for the SFPG case. From the previous discussion, we see that this is because the SFPG case represents a closer approximation to the assumption that $A=C$. For the streamwise variation in δ, the agreement is generally good, with the exception of the SFPG case where (17) predicts a decrease in wake width instead of the experimentally observed parallel flow. From relations (17) and (18) one can obtain the predicted streamwise variation of the ratio U_d/δ as

$$\frac{U_d}{\delta}=\frac{1}{1+2(T^*-T_0^*)}\left(\frac{U_{d0}}{\delta_0}\right), \tag{20}$$

which is compared with experimental results in Fig. 10. The predictions are in general agreement with the measurements.

In order to investigate the suitability of relations (17) and (18) to applications involving much stronger streamwise strain rates, we next compare their prediction with the DNS simulation results for a temporally evolving, strained planar

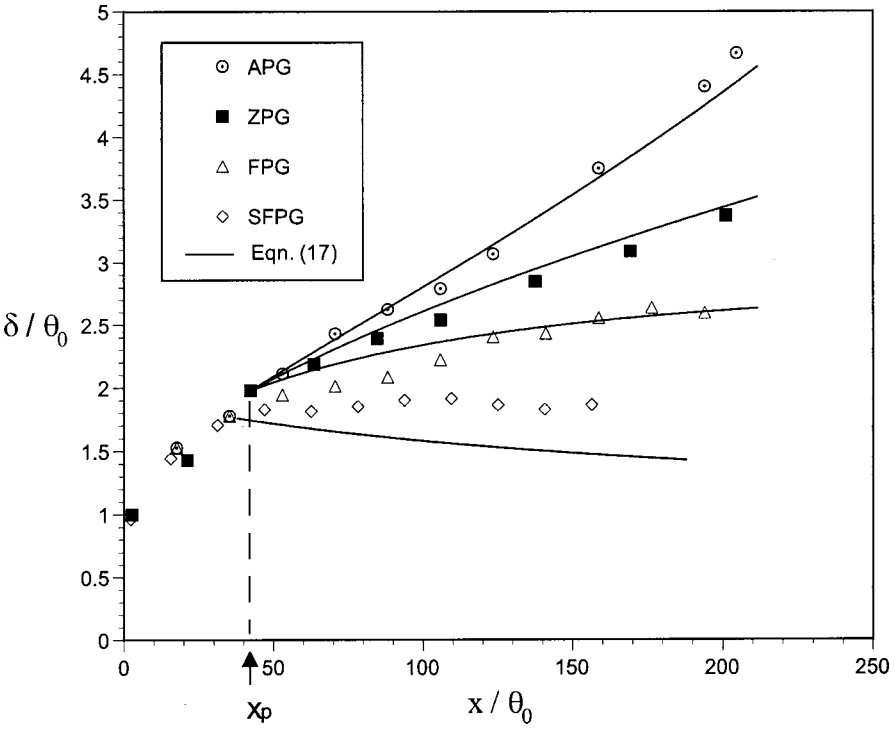

FIG. 24. Comparison of the measured and the predicted wake half-width in APG, ZPG, FPG, and SFPG.

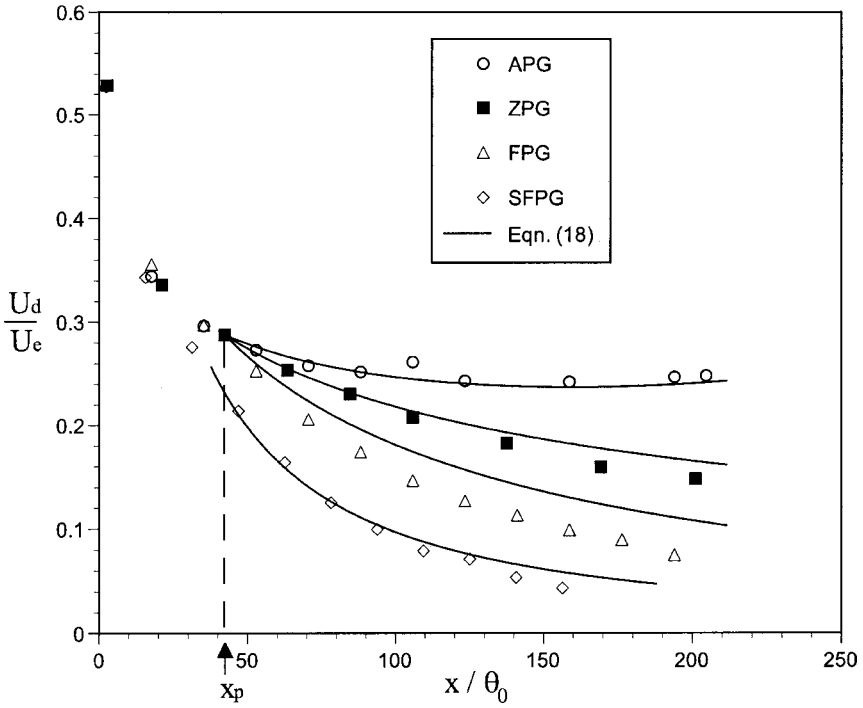

FIG. 25. Comparison of the measured and the predicted maximum velocity defect in APG, ZPG, FPG, and SFPG.

turbulent wake reported by Rogers.[19] In particular, we focus on cases that Rogers designates as C and D in which the wake is exposed to constant nondimensional streamwise strain rates of $\bar{a}=-0.271$ and $\bar{a}=+0.271$ [where $\bar{a}=(2\delta_0/U_{d0})(dU_e/dx)$]. The negative strain rate employed by Rogers is an order of magnitude larger than that encountered in our wake experiment. For example, the equivalent nondimensional strain $\bar{a}$ for the APG and FPG cases studied here are only approximately -0.01 and $+0.1$, respectively, at the location corresponding to the beginning of imposition of the pressure gradient. Since the simulations of Rogers involve a temporally evolving turbulent wake, relations (17) and (18) must be transformed to the equivalent temporally evolving form. This gives, when both dU_e/dx and K are taken as constants,

$$\frac{\delta(\tau)}{\delta(\tau_0)}=\frac{\sqrt{1+4K(\tau-\tau_0)}}{e^{\bar{a}(\tau-\tau_0)}}, \tag{21}$$

$$\frac{U_d(\tau)}{U_d(\tau_0)}=\frac{1}{e^{\bar{a}(\tau-\tau_0)}\sqrt{1+4K(\tau-\tau_0)}}, \tag{22}$$

where

$$\tau-\tau_0=\frac{U_{d0}}{2\delta_0}\int_{x_0}^{x}\frac{dx}{U_e(x)}. \tag{23}$$

The temporal evolution of δ and U_d predicted by relations (21) and (22) is compared with Rogers DNS results in Figs. 26 and 27, respectively. In order to assess the sensitivity of the comparison to the assumed constant value of K, the comparison is made for both $K=0.044$ (the same value used in the previous comparisons with experiment) and $K=0.014$. For the accelerated wake flow ($\bar{a}=+0.271$) Figs. 26 and 27 show that the comparison is not very sensitive to the choice of K. In contrast, the decelerated wake flow ($\bar{a}=-0.271$) is more sensitive to the choice of K. Although the trends are well captured for $K=0.044$, deviations between predicted and actual values of δ and U_d emerge, particularly at large times τ. For the decelerated wake, the prediction based on relations (21) and (22) with $K=0.014$ shows quite good agreement with the DNS results even at large values of τ.

The comparisons with both experimental and DNS results suggest that K is a fairly weak function of pressure gradient and that with suitable ''calibration,'' relations (17) and (18) should be capable of providing very good estimates of δ and U_d in even large adverse pressure gradient environments. For favorable pressure gradients the predictive ability of relations (17) and (18) is less impressive and appears comparatively insensitive to the choice of the value of parameter K. In particular, the prediction for the FPG case underestimates the defect decay rate and overestimates the decrease of the wake width. This may reflect an inherent limitation of the analysis which is based upon the assumption of incomplete flow similarity. Fortunately, for high-lift applications, wake development occurs primarily in a strong adverse pressure gradient environment where relations (17) and (18) appear capable of providing good predictions.

Finally, it should be noted that forming the product $U_d(\tau)\delta(\tau)$ from relations (21) and (22), respectively, yields

$$U_d(\tau)\delta(\tau)=U_d(\tau_0)\delta(\tau_0)e^{-2\bar{a}(\tau-\tau_0)}, \tag{24}$$

which is identical to the expression derived by Rogers[19] from cross-stream integration of the momentum equation for the temporally evolving wake flow subjected to constant strain rate. Essentially relation (24) is equivalent to

$$U_e^2U_d(\tau)\delta(\tau)=U_{e0}^2U_d(\tau_0)\delta(\tau_0)=M=\text{const} \tag{25}$$

if the key transformation relation between the temporal and spatial domains $U_e=U_{e0}+a(x-x_0)$ is valid. Relation (25)

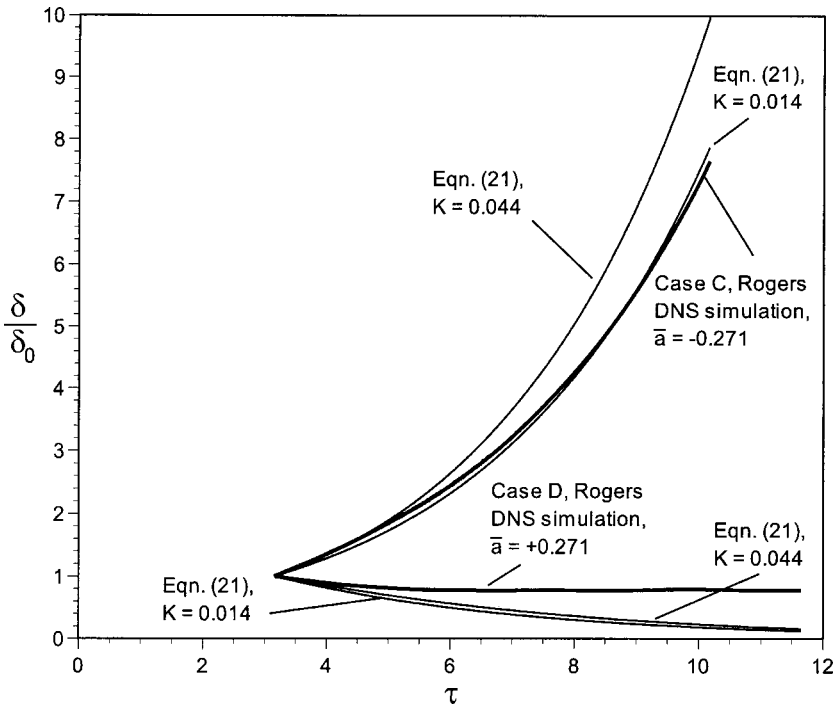

FIG. 26. Comparison of the predicted wake half-width with the DNS results of Rogers (Ref. 19).

states that the mean flow kinetic energy defect is a constant for the temporally evolving wake flow subjected to constant strain rate as simulated by Rogers.[19]

VI. DISCUSSION

The experimental results demonstrate that even modest pressure gradients have a large influence on both wake spreading and velocity defect decay rate. When the adverse pressure gradient is imposed, the wake spreading rate is enhanced, the velocity defect decay rate is reduced, and the turbulence intensity and the Reynolds stress are both amplified. In contrast, when the wake develops in a favorable pressure gradient, the wake spreading rate is reduced, the velocity defect decay rate is increased, and the turbulence intensity and Reynolds stress are both decreased in relation to corresponding zero pressure gradient values. The experiments show that the response of the wake mean flow to the imposed pressure gradient is very rapid while the turbulence is considerably slower to respond. The sensitivity of the wake mean flow to the imposed pressure gradient is not symmetric

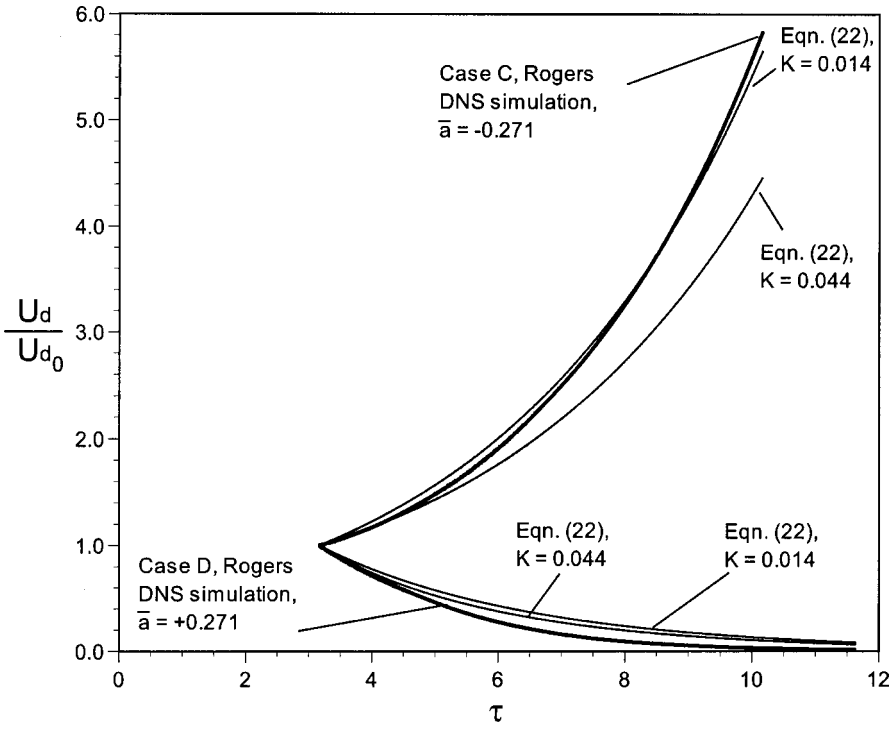

FIG. 27. Comparison of the predicted maximum velocity defect with the DNS results of Rogers (Ref. 19).

relative to the zero pressure gradient condition; the response of the mean flow is more sensitive to adverse pressure gradients.

Despite the demonstrated sensitivity of δ and U_d to the imposed pressure gradients, the experiments show that the wake mean velocity defect profiles for the APG, ZPG, FPG, and SFPG cases all collapse to a common shape for $x/\theta_0 > 40$ when scaled by δ and U_d. In his DNS simulations of a planar turbulent wake exposed to constant rates of streamwise straining, Rogers[19] also noted a universal wake profile shape. Our experiment also showed that the ratio U_d/δ exhibits a streamwise variation that is nearly identical for each of the pressure gradient cases. This, along with the common wake defect profile shape, indicates that the mean strain rate $\partial\overline{U}/\partial y$ at corresponding y/δ locations is unaffected by the applied pressure gradients.

The experiments also demonstrate that the spreading of the wake in $\psi - x$ space is invariant with respect to the imposed pressure gradient. In addition, the ψ value corresponding to a fixed y/δ is not constant, which indicates that the wake boundary does not simply follow the streamlines of the external inviscid flow.

An analysis that exploits the incomplete similarity observed in the wake experiments yields explicit analytical expressions for $\delta(x)$ and $U_d(x)$. Comparison of the theoretical prediction with the experimental data shows that expressions (17) and (18) capture the essential aspects of the streamwise variation of global mean flow parameters. The agreement is best for the APG case and worse for favorable pressure gradients. Their ability to predict wake development in much stronger pressure gradients was verified by comparing the expressions (transformed to the temporal domain) with Rogers' DNS simulation results for a temporally evolving, strained planar wake. This comparison showed that if properly calibrated, the relations are capable of capturing the wake mean flow parameters in pressure gradients much larger than those encountered in our experiments. This is particularly true for negative strain rates. In addition, expressions (21) and (22) yield an expression for $U_d\delta$ which is identical to the one derived by Rogers[19] in the temporal domain.

The similarity of the wake flow in the near-field is incomplete since the profiles of normal and Reynolds shear stresses do not exhibit similarity if scaled by δ and U_d. However, if the Reynolds shear stress $-\overline{u'v'}$ is decomposed into an x-dependent amplitude function $G_{uv}(x)$ and a lateral shape function $g(\eta)$, it is found that the shape function $g(\eta)$ is identical in all pressure gradient cases. However, for the normal stress $\overline{u'^2}$, no such universal shape function $h(\eta)$ is observed.

In addition to modifying the turbulence kinetic energy levels in the wake, the pressure gradient also effects the rate at which profiles of second-order turbulence statistics approach similarity. Experimental results show that for the adverse pressure gradient, the approach of turbulence quantities to self-similarity is significantly accelerated over that observed for the zero pressure gradient case. In contrast, for the applied favorable pressure gradients, scaled profiles of turbulent quantities do not exhibit collapse.

Cross-stream profiles of $-\overline{u'v'}/k$ obtained at various streamwise locations exhibit collapse for each pressure gradient case investigated. This suggests the suitability of Rodi's weak equilibrium assumption and the applicability of algebraic stress models for this class of strained flows. These experimental results also imply that the components of the Reynolds-stress anisotropy tensor are largely invariant with respect to mean flow convection.

The wakes studied in this paper are all shear dominated despite the imposed streamwise straining. However, the dilatational production term is found to play an important role in augmenting and suppressing the turbulence for the APG and FPG cases, respectively. Acting as a trigger, this term gives rise to the initial disparity in turbulence levels after imposition of the pressure gradients and subsequently alters the shear production term through modification of $-\overline{u'v'}$. Measurements of the Reynolds stress correlation suggest no significant modification in the phase relationship between u' and v' due to the imposed pressure gradients.

In these experiments, the magnitude of the imposed pressure gradients was limited by a desire to achieve constant pressure gradients in the diffuser section. It may be shown that for the range of flow velocities encountered in the experiment, the streamwise strain rate is nearly constant as was the case in the DNS simulations of Rogers.[19] In an actual high-lift system, however, the pressure gradient magnitudes are significantly larger and vary in the streamwise direction. For example, a slat wake typically encounters a short duration favorable pressure gradient followed by a strong and spatially varying adverse pressure gradient. This gives rise to a highly nonequilibrium turbulent wake flow where there may be little direct relation between local mean strain rate and Reynolds stress. In other words, ''memory'' effects associated with the upstream flow history may become far more important. One way to impose a pressure field that more closely resembles that which occurs in an actual high-lift system would be to pass the splitter plate wake through the pressure distribution generated by a single downstream airfoil or between a twin airfoil configuration. As in an actual high-lift system, the wake would initially encounter a short duration favorable pressure gradient and this would be followed, in turn, by a more extended region of adverse gradient. In addition, the associated strain rate variation in the streamwise direction would be quite significant giving rise to a highly nonequilibrium turbulent wake flow that is analogous to that encountered in a high-lift system. Such experiments are currently underway in our laboratory.

ACKNOWLEDGMENTS

This research was supported by NASA Langley Research Center, Hampton, VA, under Grant No. NASA-NAG1-1987. The experiment has greatly benefited from discussions with Ben Anders, Christopher Rumsey, John Carlson, and William L. Sellers III of NASA Langley Research Center and Michael M. Rogers of NASA Ames Research Center. Technical support from Michael M. Rogers,

TABLE I. Wall contour coordinates for adverse, zero, favorable, and strong favorable pressure gradient cases.

x_w (cm)	APG y_w (mm)	ZPG y_w (mm)	FPG y_w (mm)	SFPG y_w (mm)
0.0	0.0	0.0	0.0	0.0
5.1	0.0	−0.4	0.0	0.0
25.4	−3.0	−3.4	0.0	−2.0
45.7	−10.5	−3	8.0	22.0
66.0	−20.5	−3	14.0	41.0
86.4	−28.5	−4.5	22.0	52.0
106.7	−40.0	−5.5	26.0	63.0
129.5	−57.0	−6.5	31.0	71.0
163.8	−83.5	−3.5	44.0	84.0

who provided DNS data for comparison, is gratefully acknowledged. We would also like to acknowledge the development of an early version of the similarity analysis by Andrey Gordeyev.

APPENDIX: DIFFUSER WALL COORDINATES

The wall contour coordinates corresponding to each of the pressure gradient cases are shown in the Table I. In Table I, x_w is the abscissa of the wall coordinates in the streamwise direction and y_w denotes the ordinate of the wall in the cross-stream direction. The origin of the wall coordinates is located on the wall at the same streamwise location as that of the trailing edge of the splitter plate. For the position of the trailing edge of the splitter plate, please refer to the sketch of the test section as shown in Fig. 2. The wall boundary layer thickness at the location of the splitter plate trailing edge is 19 mm for APG, ZPG, and FPG cases.

[1]P. L. Garner, P. T. Meredith, and R. C. Stoner, ''Areas for CFD development as illustrated by transport aircraft applications,'' AIAA Pap. 91-1527 (1991).
[2]J. C. Lin, S. K. Robinson, and R. J. McGhee, ''Separation control on high Reynolds number multi-element airfoils,'' AIAA Pap. 92-2636 (1992).
[3]A. M. O. Smith, ''High-lift aerodynamics,'' AIAA J. Aircraft **12**, 501 (1975).
[4]P. G. Hill, U. W. Schaub, and Y. Senoo, ''Turbulent wakes in pressure gradients,'' J. Appl. Mech. **30**, 518 (1963).
[5]A. V. Petrov, ''Certain types of separated flow over slotted wings,'' Fluid Mech.-Sov. Res. **7**, 80 (1978).
[6]V. D. Chin, D. W. Peters, F. W. Spaid, and R. J. McGhee, ''Flowfield measurements about a multi-element airfoil at high Reynolds numbers,'' AIAA Pap. 93-3137 (1993).
[7]S. E. Rogers, ''Progress in high-lift aerodynamic calculations,'' AIAA Pap. 93-0194 (1993).
[8]R. Hoffenberg, J. P. Sullivan, and S. P. Schneider, ''Wake measurements in a strong adverse pressure gradient,'' AIAA Pap. 95-1912 (1995).
[9]R. Hoffenberg and J. P. Sullivan, ''Measurement and simulation of a decelerated wake,'' AIAA Pap. 98-0522 (1998).
[10]M. J. Tummers, D. M. Passchier, and R. A. W. M. Henkes, ''Experimental investigation of an adverse pressure gradient wake and comparison with calculations,'' Exp. Therm. Fluid Sci. **14**, 17 (1997).
[11]F. W. Roos, ''Experimental studies of wake retardation in a simulated high-lift system flow field,'' AIAA Pap. 97-1813 (1997).
[12]D. M. Driver and G. M. Mateer, ''Wake flow in adverse pressure gradient,'' Paper 2000-01-5511, SAE/AIAA World Aviation Congress and Exposition, San Diego, CA, 2000.
[13]R. Narasimha and A. Prabhu, ''Equilibrium and relaxation in turbulent wakes,'' J. Fluid Mech. **54**, 1 (1972).
[14]A. Prabhu and R. Narasimha, ''Turbulent non-equilibrium wakes,'' J. Fluid Mech. **54**, 19 (1972).
[15]A. J. Reynolds, ''Observation on distorted turbulent wakes,'' J. Fluid Mech. **13**, 333 (1962).
[16]J. F. Keffer, ''The uniform distortion of a turbulent wake,'' J. Fluid Mech. **22**, 135 (1965).
[17]I. S. Gartshore, ''Two-dimensional turbulent wakes,'' J. Fluid Mech. **30**, 547 (1967).
[18]A. Nakayama, ''Curvature and pressure-gradient effects on a small-defect wake,'' J. Fluid Mech. **175**, 215 (1987).
[19]M. M. Rogers, ''The evolution of strained turbulent plane wakes,'' J. Fluid Mech. **463**, 53 (2002).
[20]X. Liu, F. O. Thomas, and R. C. Nelson, ''An experimental investigation of wake development in arbitrary pressure gradients,'' AIAA Pap. 99-0677 (1999).
[21]P. S. Klebanoff, ''Characteristics of turbulence in a boundary layer with zero pressure gradient,'' NACA TN 3178 (1954).
[22]H. Schlichting, *Boundary Layer Theory*, 7th ed. (McGraw–Hill, New York, 1979).
[23]I. Wygnanski, F. Champagne, and B. Marasli, ''On the large-scale structure in two-dimensional, small-Deficit, turbulent wakes,'' J. Fluid Mech. **168**, 31 (1986).
[24]F. O. Thomas, R. C. Nelson, and X. Liu, ''Experimental investigation of the confluent boundary layer of a high-lift system,'' AIAA J. **36**, 978 (2000).
[25]W. K. George, ''The self-preservation of turbulent flows and its relation to initial conditions and coherent structures,'' in *Advances in Turbulence*, edited by W. K. George and R. Arndt (Hemisphere, New York, 1989).
[26]S. B. Pope, *Turbulent Flows* (Cambridge University Press, New York, 2000).
[27]X. Liu, ''A study of wake development and structure in constant pressure gradients,'' Ph.D. dissertation, University of Notre Dame, 2001.